Walport, F., Gardner, L., and Nethercot, D.A. (2021). Design of structural stainless steel members by second order inelastic analysis with CSM strain limits, *Thin-Walled Structures*, 159, 107267.

Design of structural stainless steel members by second order inelastic analysis with CSM strain limits

F. Walport, L. Gardner and D.A. Nethercot

Imperial College London, London, UK

E-mails: fiona.walport12@imperial.ac.uk, leroy.gardner@imperial.ac.uk, d.nethercot@imperial.ac.uk

Abstract: *System-level advanced analysis is now a viable tool for widespread use in structural design. By directly capturing frame and member level instability effects, plasticity, initial geometric imperfections and residual stresses in the analysis, the need for subsequent individual member checks can be eliminated. The analysis of structural members and frames is typically carried out using beam elements, which are unable to capture the effects of local buckling. However, local buckling dictates the strength and ductility of cross-sections and the extent to which plastic redistribution of forces and moments can be exploited; it cannot therefore be disregarded. A proposal is made herein, in which strain limits, defined by the continuous strength method, are applied to simulate local buckling in beam element models, thereby controlling the degree to which spread of plasticity, force and moment redistribution and strain hardening can be utilised in the design of structural elements and systems. Strains are averaged over a defined distance along the member length to reflect the fact that local buckling requires a finite length over which to develop and to allow for local moment gradient effects. Design is based directly on the application of strain limits to all cross-sections in the structure. The accuracy of the proposed method for the design of stainless steel members is assessed through comparisons with benchmark shell finite element results; both I-section and* *hollow section members are considered. Comparisons against current design methods confirm the significant benefits of applying the proposed approach in terms of both the accuracy and the consistency of the resistance predictions. The reliability of the design approach is demonstrated through statistical analyses performed in accordance with EN 1990. Application of the proposed method is particularly appropriate for stainless steel structures due to the high material value and the complexities presented by the nonlinear material stress–strain response for traditional design treatments. The proposed method is due to be included in the two major international stainless steel design standards EN 1993-1-4 and AISC 370.*

Keywords: Advanced analysis; Continuous strength method; Equivalent imperfections; Global analysis; Inelastic analysis; Local buckling; Nonlinear analysis; Plastic zone analysis; Second order effects; Stainless steel; Strain limit.

1. INTRODUCTION

Stainless steel has a relatively high initial cost compared to carbon steel and it is therefore important that design rules enable the material to be utilised to the fullest by recognising its particular features, as well as by embracing advanced design methods that may deviate from traditional approaches. With advances in computational power and software, system-level advanced (second order) inelastic analysis is now viable for widespread use in design [1]. The nonlinear material behaviour of stainless steel results in added complexities for traditional design, and makes the opportunities offered by more advanced techniques particularly advantageous. Second order inelastic analysis enables the distribution of internal forces and moments within a structure to be accurately determined since the erosion of stiffness due to buckling and plasticity is directly modelled [2]. Advanced analysis is commonly carried out using beam element finite element models which are incapable of capturing the effects of local buckling directly since cross-section deformation is not possible. However, disregarding local buckling can lead to overestimations of cross-section capacities and hence system strengths. This is of particular concern for stainless steel due to the nonlinear stress–strain response and the significant development of strain hardening; cross-section capacities, therefore, continuously increase under increasing deformation and do not plateau at the traditional plastic moment capacity. Shell finite element models are able to accurately capture all cross-section behaviour but are considerably more computationally expensive than beam elements. A design approach is presented herein that utilises beam elements, yet safely captures cross-section failure across the full local slenderness range through the continuous strength method (CSM). The CSM is employed to simulate local buckling by applying strain limits to all the cross-sections within the member or structure, thereby controlling the extent to which plasticity, moment redistribution and strain hardening can be exploited. This method has previously been developed and applied to carbon steel structures [3–5] and is extended to stainless steel in this study. An alternative approach is to simulate local buckling by defining an effective stress-strain curve that is a function of the cross-section geometry and loading conditions [6,7]. The present paper outlines the proposed approach for the in-plane design of structural stainless steel members subjected to bending, compression and combined loading, with the accuracy assessed against benchmark shell finite element models; comparisons are also made against current Eurocode design predictions.

2. CURRENT EUROCODE PROVISIONS

EN 1993-1-4 [8] provides supplementary rules, beyond those set out in EN 1993-1-1 [9] for carbon steel, for the design of stainless steel structures. However, for frame stability and structural analysis, no further guidance is currently given. The effect of the characteristic rounded stress–strain curve of stainless steel is therefore ignored in this crucial aspect of structural design. The consequences of this were assessed in a study by Walport et al. [10], where it was concluded that the material nonlinearity of stainless steel results in greater deflections due to the loss of material stiffness and therefore, without due consideration, forces and moments are generally underestimated. It was recommended that material nonlinearity should always be considered in the global analysis of stainless steel structures, unless the structure remains predominantly in the elastic range.

Traditional design methods, including those set out in EN 1993-1-1 [9] are based on the assignment of cross-sections to discrete behavioural classes. Each class represents an idealised cross-section response; whether the cross-section possesses sufficient rotation capacity to allow the application of plastic analysis and design is also defined. In the case of bending, Class 1 cross-sections can reach their full plastic moment capacity M_{pl} and are deemed to have sufficient rotation capacity for plastic design. Class 2 cross-sections can attain their plastic moment capacity but have insufficient ductility for plastic design. Class 3 cross-sections are limited to their elastic moment capacity M_{el} and Class 4 cross-sections an effective moment capacity M_{eff}. This cross-section classification framework has two key limitations when applied to stainless steel design. Firstly, in stainless steel structures, plastic redistribution occurs at relatively low load levels due to the rounded stress–strain response of the material – not only is this issue ignored in the current design provisions (EN 1993-1-4), it is also exacerbated by not allowing plastic analysis, even for Class 1 cross-sections. Secondly the cross-section resistance in bending is limited to the plastic moment capacity M_{pl}; this disregards the substantial strain hardening of stainless steel, often resulting in very conservative design solutions. Material nonlinearity results in added complexities for traditional design approaches and therefore the opportunities of design by advanced analysis should be exploited, as presented herein.

3. BENCHMARK SHELL FINITE ELEMENT MODELLING

Benchmark shell finite element (FE) models of stainless steel beams, columns and beam-columns are used in this study to assess the accuracy of both the proposed design approach presented in Section 4 and the current Eurocode design provisions. The FE models were developed using the general purpose FE software Abaqus [11]; the general modelling approach and validation are presented in this section, while the results are utilised in Section 4.

3.1. Modelling approach

For the benchmark modelling, geometrically and materially nonlinear shell finite element analyses with imperfections (GMNIA) were performed. The four-noded reduced integration S4R shell element, from the Abaqus element library [11], was employed to create the models and used in all benchmark simulations. Both welded I-sections and cold-formed hollow sections were modelled, with the web depth and flange width subdivided into 12 elements to accurately capture local buckling (both in the elastic and inelastic ranges). The number of elements along the length of the member was defined such that the aspect ratio of the elements remained close to unity. The modified Riks method was used to trace the full load-deformation response of the members.

The rounded stress–strain response of stainless steel, defined on the basis of the two-stage Ramberg–Osgood formulation [12–15] and further described in Section 4.1.2, was incorporated into the shell FE models. Note that the Ramberg–Osgood formulation presents strains as a function of stress; while this can be problematic for analytical solutions and for some software, in the case of most FE software, the Ramberg–Osgood model can be readily incorporated by converting the continuous function into a multi-linear representation. In the present study the stress–strain curves were defined by 135 steps for an accurate representation of the material behaviour. The engineering stress–strain curves were converted into true stress–strain curves for compatibility with the adopted element type (S4R [11]) in which changes in cross-sectional area during the geometrically nonlinear analyses are captured. For the welded I-sections, the ECCS [16] residual stress pattern, as modified for stainless steel by Yuan et al. [17], was introduced into the FE models by defining an initial stress condition. Corresponding plastic strains were also assigned [18] and a preliminary analysis step was employed prior to the application of external loading to allow the residual stresses to equilibrate. For the cold-formed hollow sections, residual stresses were not explicitly introduced; this is because the influence of the dominant through thickness residual stresses are already present in the material stress–strain curves obtained from tests on coupons extracted from cold-formed hollow sections [19] and because their influence on the structural behaviour of cold-formed stainless steel tubular members have generally been found to be small [20,21]. Sinusoidal local plate imperfections were defined with an imperfection magnitude of 1/200 times the plate width, as recommended in EN 1993-1-5 [22], and a length close to the local buckling half-wavelength of the cross-section $L_{b,cs}$ calculated from a finite strip analysis in CUFSM [23]. Simplified formulae for the calculation of local buckling half-wavelengths have also been established [24].

Pin and roller support conditions were achieved through the coupling of all nodes of the member end cross-sections to a master node and the application of suitable boundary conditions to that node. The members were restrained out-of-plane along the flange centrelines at intervals close to the local buckling half-wavelength $L_{b,cs}$ since in-plane stability design is the focus of the present paper. Concentrated loads were applied at the bottom of the web and web stiffeners with a thickness equal to the web thickness were included in the models at the load locations to prevent localised web failure.

3.2. Validation

The shell FE models were validated against the results of 91 experiments on stainless steel I-section and square/rectangular hollow section (SHS/RHS) members from the literature. Different loading configurations were considered, including beams in three- and four-point bending [25–27], columns of varying slenderness [27–29] and beam-columns [29–31].

The measured cross-section geometry, material properties and imperfection magnitudes from the tests were used as input parameters for the FE validation models. Where available, different material properties were applied to the flanges and web of the welded I-sections. For the hollow sections, the rounded corner geometry was modelled explicitly with five elements in each corner; also, enhanced corner material properties, owing to the effect of work hardening, were assigned to the curved corner regions plus an extension of $2t$, where t is the material thickness, in accordance with the findings of [32].

A summary of the shell FE model validation, including the mean and coefficient of variation (COV) of the shell FE model to test failure load ratios, is given in Table 1. Generally, the shell FE models were able to accurately predict the experimental failure loads for both the I-section and SHS/RHS members, with an overall average FE-to-test ultimate load ratio of 1.00 and a corresponding COV of 0.057.

Figures 1 and 2 show typical load–deformation curves obtained from tests [25,31] and the shell FE models for I-sections under three-point bending (3PB) and SHS/RHS under combined bending and compression, respectively. The numerical simulations can be seen to be in close agreement with the observed physical behaviour. Overall, the FE models are therefore considered to provide reliable results against which the proposed design method can be benchmarked.

4. DESIGN BY SECOND ORDER INELASTIC ANALYSIS USING BEAM FINITE ELEMENTS WITH STRAIN LIMITS

In this section, a method of design by second order inelastic analysis using beam finite element models with strain limits is developed. To simulate local buckling in the beam element models, the continuous strength method (CSM) has been utilised. The continuous nature of the approach allows cross-sections of all classes to be designed in a consistent manner. Failure of a member or structure is defined as the first to occur of (1) the CSM strain limit is reached or (2) the peak load is attained [10]. The latter criterion is typically critical in stability governed scenarios.

4.1. The continuous strength method

The continuous strength method (CSM) is a deformation-based method that replaces the earlier described concept of cross-section classification with a continuous relationship between cross-section slenderness and deformation (strain) capacity [33–35]. The CSM has two key components (1) a continuous 'base curve' determining the maximum strain ε_{csm} that a cross-section can withstand under the applied loading, and (2) a constitutive model to capture the nonlinear stress–strain characteristics of the material. In this study it is the first component that will be utilised to simulate local buckling by limiting strains in the beam elements models. This approach is described in the following subsections.

4.1.1. Base curve

The base curve defines the maximum strain ε_{csm} that a cross-section of a given local slenderness $\bar{\lambda}_p$ can withstand prior to failure. The base curve implicitly includes the influence of local geometric imperfections and residual stresses on the cross-section response. For use in manual design calculations, in conjunction with a simplified elastic, linear hardening material model, the CSM base curve is given by Eqs. (1) and (2), where $\bar{\lambda}_{\mathrm{p}}$ is the local cross-sectional slenderness discussed later, ε_{y} is the yield strain equal to the yield stress f_{y} divided by the Young's modulus E, ε_{u} is the ultimate strain estimated as $\varepsilon_{\mathrm{u}}=1-f_{\mathrm{y}}/f_{\mathrm{u}}$ for austenitic and duplex stainless steel and as $\varepsilon_{\mathrm{u}}=0.6(1-f_{\mathrm{y}}/f_{\mathrm{u}})$ for ferritic stainless steel, where f_{u} is the ultimate stress, and C_1 is a coefficient equal to 0.1 for austenitic (A) and duplex (D) stainless steels and 0.4 for ferritic (F) stainless steels [34,36]. Eq. (1) defines the CSM strain limit for non-slender cross-sections while Eq. (2) defines the CSM strain limit for slender cross-sections, where local buckling occurs prior to reaching the yield resistance. Two upper limits are included in Eq. (1): the first, Ω (denoted Λ in AISC 370 [37]), is a project specific design parameter that defines the maximum allowable level of plastic deformation [3] while the second, $C_1\varepsilon_{\mathrm{u}}/\varepsilon_{\mathrm{y}}$, prevents overpredictions of material strength when using the CSM for hand calculations with a simplified elastic, linear hardening stress–strain model. In this study values of Ω=15 (generally recommended to prevent excessive deformations) and Ω=30 are considered.

$$\frac{\varepsilon_{\mathrm{csm}}}{\varepsilon_{\mathrm{y}}}=\frac{0.25}{\bar{\lambda}_{\mathrm{p}}^{3.6}} \quad \text{but} \quad \leq \left(\Omega, \frac{C_1\varepsilon_{\mathrm{u}}}{\varepsilon_{\mathrm{y}}}\right) \quad \text{for} \quad \bar{\lambda}_{\mathrm{p}} \leq 0.68 \tag{1}$$

$$\frac{\varepsilon_{\mathrm{csm}}}{\varepsilon_{\mathrm{y}}}=\left(1-\frac{0.222}{\bar{\lambda}_{\mathrm{p}}^{1.05}}\right)\frac{1}{\bar{\lambda}_{\mathrm{p}}^{1.05}} \quad \text{for} \quad 0.68<\bar{\lambda}_{\mathrm{p}} \leq 1.6 \tag{2}$$

To facilitate hand calculations, the CSM employs an elastic, linear hardening material model [34] in conjunction with Eqs. (1) and (2), as indicated above. However, for design by second order inelastic analysis of stainless steel structures, which is the focus of the present study, the more accurate two-stage Ramberg–Osgood material model [14] described in Section 4.1.2 can be used since the necessary computations are performed numerically; this difference in material model requires an adjustment to the CSM base curves. Eqs. (3) and (4) describe the adjusted CSM base curves for use in second order inelastic analysis with the two-stage Ramberg–

Osgood material model for non-slender and slender cross-sections, respectively. Essentially, to account for the difference between the bilinear and rounded stress–strain curves, a constant strain of 0.2% is added to the base curve for $\bar{\lambda}_{\mathrm{p}} \leq 0.68$, while a stress-level dependent strain is added in the slender range (i.e. $\bar{\lambda}_{\mathrm{p}} > 0.68$). The modifications from Eqs. (1) and (2) to Eqs. (3) and (4) are illustrated in Figure 3.

$$\frac{\varepsilon_{\mathrm{csm}}}{\varepsilon_{\mathrm{y}}} = \frac{0.25}{\bar{\lambda}_{\mathrm{p}}^{3.6}} + \frac{0.002}{\varepsilon_{\mathrm{y}}} \quad \text{but} \quad \leq \Omega \quad \text{for} \quad \bar{\lambda}_{\mathrm{p}} \leq 0.68 \tag{3}$$

$$\frac{\varepsilon_{\mathrm{csm}}}{\varepsilon_{\mathrm{y}}} = \left(1 - \frac{0.222}{\bar{\lambda}_{\mathrm{p}}^{1.05}}\right) \frac{1}{\bar{\lambda}_{\mathrm{p}}^{1.05}} + \frac{0.002\left(\sigma/f_{\mathrm{y}}\right)^{n}}{\varepsilon_{\mathrm{y}}} \quad \text{for} \quad 0.68 < \bar{\lambda}_{\mathrm{p}} \leq 1.0 \tag{4}$$

where σ is the maximum compressive stress, f_{y} is the yield (0.2% proof) stress and n is the strain hardening exponent defined in Section 4.1.2. Note that the range of applicability of Eq. (4) is reduced relative to Eq. (2) (from $\bar{\lambda}_{\mathrm{p}}$ = 1.6 to $\bar{\lambda}_{\mathrm{p}}$ = 1.0), since Eq. (2) is used for checking individual members for which it has been extensively verified [38], while Eq. (4) can be applied to complete structural systems. For structural systems comprising members with slender cross-sections, the loss of stiffness associated with local buckling can affect the distribution of forces and moments around the frame, which may require specific attention either through a reduced stiffness approach [39] for beam elements or through explicit modelling using shell elements.

The cross-section slenderness $\bar{\lambda}_{\mathrm{p}}$ quantifies the susceptibility of a cross-section to local buckling and is calculated using Eq. (5), where $\sigma_{\mathrm{cr,cs}}$ is the local elastic buckling stress of the full cross-section. This can be obtained either using numerical methods e.g. CUFSM [23] or using the simplified expressions of Gardner et al. [40].

$$\bar{\lambda}_{\mathrm{p}} = \sqrt{\frac{f_{\mathrm{y}}}{\sigma_{\mathrm{cr,cs}}}} \tag{5}$$

4.1.2. Material model

The rounded stress–strain response of stainless steel is described on the basis of the two-stage Ramberg–Osgood formulation [14,15], as given by Eqs. (6) and (7), and included in prEN 1993-1-14 [41], where ε and σ are the strain and stress, respectively, E is the Young's modulus, f_u is the ultimate stress, E_y is the tangent modulus at the 0.2% proof stress, defined by Eq. (8), $\varepsilon_{0.2}$ is the total strain at the 0.2% proof stress, equal to 0.002 + f_y/E, ε_u is the ultimate strain, and n and m are the strain hardening exponents.

$$\varepsilon = \frac{\sigma}{E} + 0.002\left(\frac{\sigma}{f_y}\right)^n \quad \text{for} \quad \sigma \le f_y \tag{6}$$

$$\varepsilon = \varepsilon_{0.2} + \frac{\sigma - f_y}{E_y} + \left(\varepsilon_u - \varepsilon_{0.2} - \frac{f_u - f_y}{E_y}\right)\left(\frac{f - f_y}{f_u - f_y}\right)^m \quad \text{for} \quad f_y < \sigma \le f_u \tag{7}$$

$$E_y = \frac{E}{1 + 0.002n\,E/f_y} \tag{8}$$

In this study, the standardised material properties for numerical parametric studies defined by Afshan et al. [42] have been employed, as summarised in Table 2. For the hollow sections, weighted average properties for each cross-section were calculated from the flat and corner properties given in Table 2 [32].

4.2. Strain averaging approach

In the proposed design approach, outer-fibre compressive strains obtained from beam FE models, ε_{Ed}, are checked against the CSM strain limits ε_{csm}, defined by Eqs. (3) and (4) to simulate the effects of local buckling, as given by Eq. (9). The member or structural resistance shall satisfy the requirements of Eq. (10), where $F_{Rd} = F_{Rk}/\gamma_{M1}$ and F_{Rk} is defined based on the first to occur of (1) the CSM strain limit is reached or (2) the peak load is attained.

$$\frac{\varepsilon_{\mathrm{Ed}}}{\varepsilon_{\mathrm{csm}}} \leq 1.0 \tag{9}$$

$$\frac{F_{\mathrm{d}}}{F_{\mathrm{Rd}}} \leq 1.0 \tag{10}$$

Since local buckling requires a finite length over which to develop, rather than restricting the peak compressive strain from beam FE models to the CSM strain limit, instead the CSM strain limit is applied to an average strain obtained over a characteristic length along the members. This characteristic length is taken as the elastic local buckling half-wavelength of the cross-section $L_{\mathrm{b,cs}}$ (denoted L_{el} in AISC 370 [37]) [3], as obtained numerically or using the simplified expressions given in [24]; CUFSM [23] was employed in the present paper. The value of $L_{\mathrm{b,cs}}$ also defines the maximum element length. This design method is expected to be included in the next version of the two major international stainless steel design standards, EN 1993-1-4 and AISC 370.

4.3. Shear resistance check

In the proposed approach, a separate shear resistance check, following the EN 1993-1-4 [8] recommendations, should be performed. EN 1993-1-4 [8] prescribes that the design shear force V_{Ed} at each cross-section be less than or equal to the plastic shear capacity of the cross-section $V_{\mathrm{pl,Rd}}$ given by Eq. (11), where A_{v} is the shear area of the cross-section [9] and γ_{M0} is the partial factor for cross-section resistance, with a recommended value for stainless steel of 1.1 [8].

$$V_{\mathrm{pl,Rd}} = \frac{A_{\mathrm{v}}\, {}^{f_{\mathrm{y}}}\!/\!_{\sqrt{3}}}{\gamma_{\mathrm{M0}}} \tag{11}$$

Following EN 1993-1-1 [9], for cross-sections subjected to combined bending and shear, an allowance is made for the effect of the shear force on the moment resistance. When the design shear force V_{Ed} is less than half the plastic shear capacity $V_{pl,Rd}$, the full bending moment resistance can be achieved but when V_{Ed} exceeds half the plastic shear capacity $V_{pl,Rd}$, a reduced moment resistance must be calculated with a reduced yield strength equal to $(1-\rho)f_y$ applied to the shear area, where ρ is calculated using Eq. (12).

$$\rho = \left(\frac{2V_{\mathrm{Ed}}}{V_{\mathrm{pl,Rd}}} - 1\right)^2 \tag{12}$$

As recommended for the design of steel structures by second order inelastic analysis in [3], in the approach proposed herein for stainless steel design, the influence of shear force on bending resistance is accounted for through the reduction factor ρ_{csm}, given by Eq. (13).

$$\rho_{\mathrm{csm}} = \begin{cases} 1 & \text{for} \quad V_{\mathrm{Ed}} \le 0.5V_{\mathrm{pl,Rd}} \\ \dfrac{0.5}{0.5+\rho} & \text{for} \quad V_{\mathrm{Ed}} > 0.5V_{\mathrm{pl,Rd}} \end{cases} \tag{13}$$

This reduction factor is applied to the CSM strain limit ε_{csm}. For cross-sections where the design shear force V_{Ed} exceeds half the plastic shear capacity $0.5V_{pl,Rd}$, the cross-section must satisfy the requirements of Eq. (14). Note that the shear check (i.e. $V_{Ed}/V_{pl,Rd} \le 1$) is still required in the proposed design approach. Also note that for cross-sections with slender webs, shear buckling must also be considered.

$$\frac{\varepsilon_{\mathrm{Ed}}}{\rho_{\mathrm{csm}}\varepsilon_{\mathrm{csm}}} \le 1.0 \qquad \text{for} \qquad V_{\mathrm{Ed}} > 0.5V_{\mathrm{pl,Rd}} \tag{14}$$

Figure 4 shows the effect of shear on the normalised bending capacity M_u/M_{pl}, where M_u is the moment capacity at failure and M_{pl} is the plastic moment capacity equal to the plastic section modulus W_{pl} multiplied by the yield stress f_y, of an austenitic stainless steel IPE 140 cross-section with varying member length under three-point bending. Observing the shell FE results, it can be seen that for very short member lengths, shear effects begin to dominate the beam behaviour, causing a sharp drop in bending capacity. If shear is ignored in these cases, the beam

FE models yield unconservative resistance predictions relative to the benchmark shell FE results. However, applying the shear reduction factor ρ_{csm} to the CSM strain limit, as well as the general shear check i.e. $V_{Ed}/V_{pl,Rd} \leq 1$, results in capacity predictions that are safe sided and accurate compared with the benchmark shell FE results, yet with significant capacity enhancements over the EN 1993-1-4 predictions. Similar conclusions can be drawn from Figure 5, which shows normalised moment–shear interaction data obtained from the shell FE simulations, where V_u is the ultimate FE shear capacity, for a range of austenitic stainless steel I-sections (HEA 160, 220, 280, 600, 800, 900; HEB 100, 200, 240, 300, 550, 700; HEM 240) subjected to three-point bending with varying member length L ranging from $2.5L_{b,cs}$ to $40L_{b,cs}$. In cases of very high shear, the shell FE models did not reach a peak capacity and failure was defined as the load at which the ratio of the tangent stiffness to the initial elastic stiffness of the model was equal to 0.01 [43]. Note that the level of plastic deformation is limited to Ω = 15 in the comparisons shown.

4.4. Initial geometric imperfections and residual stresses

EN 1993-1-1 [9] and prEN 1993-1-1 [44] provide equivalent bow imperfections that implicitly account for the combined effects of geometric and material (i.e. residual stresses) imperfections. These equivalent bow imperfections are for use with second order elastic analysis with a subsequent linear cross-section check; they are not, in general, appropriate for use in design by second order inelastic analysis and can give over-predictions (i.e. unconservative results) or under-predictions (i.e. conservative results) of buckling resistance depending on the form of the adopted material stress–strain curve [45]. In the case of design by second order inelastic analysis of stainless steel members and structures, the nonlinear material model results in early yielding, and use of the prEN 1993-1-1 [44] equivalent bow imperfections (determined for either a linear elastic or linear plastic cross-section check) leads to highly conservative capacity predictions. Equivalent bow imperfections for use with second order inelastic, or geometrically and materially nonlinear, analysis, have been developed by Walport et al. [45]. The normalised equivalent bow imperfection magnitude e_0/L for use in design by second order inelastic analysis is given by Eq. (15), where L is the member length and α is the imperfection factor. These equivalent imperfection magnitudes are used in the present study to account for the combined effects of geometrical imperfections and residual stresses; the influence of material yielding is directly captured in the analysis while the varying influence of residual stresses for different cross-section types and axes of buckling is, as in the case of the equivalent bow imperfections for use in second order elastic analysis [44,46], captured through the imperfection factor α.

$$\frac{e_0}{L} = \frac{\alpha}{150} \quad \text{but} \quad \frac{e_0}{L} \geq \frac{1}{1000} \tag{15}$$

Note that the equivalent bow imperfections given by Eq. (15) for use in design by second order inelastic (plastic zone, distributed plasticity and fibre) analysis were calibrated against benchmark FE ultimate loads generated using geometrically and materially nonlinear analysis with geometric imperfections of $L/1000$ and appropriate residual stresses [45].

5. APPLICATION OF PROPOSED DESIGN METHOD

The accuracy of the proposed approach of design by second order inelastic analysis with strain limits is assessed in this section for a wide range of structural stainless steel members. The beam finite element (FE) models employed to apply the design method were established in Abaqus using the 2-noded linear Timoshenko beam elements B31OS and B31 for the open (I-sections) and closed (SHS/RHS) cross-sections, respectively. Since there is no change in cross-section geometry under load for the adopted beam element type, engineering stresses and strains were incorporated into the models without the need for conversion into true stresses and strains (as required in the shell FE models described in Section 3). The beam FE models were discretised such that the element length was equal to that used in the shell FE models.

Application of the design method to members subjected to bending, compression and combined compression and bending is assessed with respect to the benchmark ultimate loads determined using the shell FE models as described in Section 3. Comparisons are also made against the results obtained using conventional Eurocode design calculations.

5.1. Members subjected to bending

Application of the proposed approach of design by second order inelastic analysis with CSM strain limits to stainless steel members subjected to bending is described in this section. Figure 6 shows the results for an example simply-supported beam under three-point bending and the application of the proposed approach. While the beam FE model continues deforming under increasing load with no peak since local buckling is not captured by this element type, the benchmark shell FE model, which does capture local buckling, fails at a peak moment. The modelled cross-section is Class 1 and therefore applying a Eurocode cross-section check results in a conservative bending resistance prediction equal to plastic moment capacity M_{pl}. For the HEA 800 cross-section considered, the cross-section slenderness in bending $\bar{\lambda}_p$ is equal to 0.34, which corresponds to a CSM strain limit $\varepsilon_{csm}/\varepsilon_y$ of 13.8 from Eq. (3); this strain limit is applied to the outer compressive fibre of the cross-section of the beam element model. As can be seen in Figure 6, adopting this approach results in a capacity prediction close to but on the safe side of the peak moment from the shell FE model, and with a 30% increase in capacity over the Eurocode prediction.

The normalised bending capacities M_u/M_{el}, where M_{el} is the elastic moment capacity equal to the elastic section modulus W_{el} multiplied by the yield stress f_y, for a series of austenitic stainless steel I-section beams subjected to three-point bending are shown in Figure 7. The local moment gradient was kept approximately constant in each member by defining the member length equal to 10 times the local buckling half-wavelength $L_{b,cs}$ for each cross-section modelled. It can be seen that the upper limit of Ω = 15 results in more conservative predictions for the stockier cross-sections and increasing this limit to Ω = 30 allows for more accurate representation of the shell FE model behaviour. Close agreement is achieved between the shell FE model results and the results from the beam FE models with CSM strain limits.

In total, over 800 simply-supported austenitic, duplex and ferritic stainless steel I-sections and hollow section beams with varying local slenderness have been assessed under three- and four-point bending. Table 3 provides a summary of the capacity predictions for both the proposed method M_{prop} (with Ω = 15) and EN 1993-1- 4 [8] M_{EC}, normalised by the benchmark shell FE results M_{shell}. The current Eurocode design provisions can be seen to be very conservative for stainless steel design, with an overall mean value of M_{EC}/M_{shell} of 0.78, while the proposed approach provides consistently more accurate capacity predictions, with an overall mean value of $M_{prop(\Omega = 15)}/M_{shell}$ of 0.93. Figure 7 illustrates the consistent and significant benefits of adopting the proposed approach over the traditional EN 1993-1-4 rules for the design of members subjected to bending.

5.2. Members subjected to compression

Application of the proposed approach of design by second order inelastic analysis with CSM strain limits to stainless steel members subjected to compression is described in this section. The assessment was carried out on 1185 pin-ended columns (591 I-section and 594 hollow section members), considering austenitic, duplex and ferritic stainless steel grades, major axis buckling, a range of cross-section slenderness values $\bar{\lambda}_p$ and three member slenderness values

($\bar{\lambda}$ = 0.5, 1.0, 1.5). A summary of the results is presented in Table 4. Ultimate buckling capacities determined using the benchmark shell FE modelling, the beam FE modelling with CSM strain limits and the traditional EN 1993-1-4 design resistance functions normalised by the plastic squash load N_{pl}, equal to the cross-section area A multiplied by the yield stress f_y, are compared in Figures 8 and 9 for austenitic stainless steel I- and hollow section columns, respectively. Note that for the design of the members with low cross-section slenderness, the peak load factor governed, while for members with slender cross-sections, the CSM strain limit was reached prior to the peak load factor being achieved.

In deriving the equivalent bow imperfections for use in design by second order inelastic analysis [45], as for second order elastic analysis [44,46,47], solutions were sought that were independent of member slenderness and therefore a level of conservatism was accepted in the predicted member capacities. This is reflected in the results shown in Figures 8 and 9 where, as observed by Walport et al. [45], it can be seen that capacity predictions from the proposed design method become more conservative as the member slenderness reduces.

An additional source of conservatism is that the first order distribution of stresses was utilised in the calculation of the cross-section slenderness (which is dependent on the elastic local buckling stress) and hence the CSM strain limit for the studied compression members; this is consistent with traditional EN 1993-1-4 design, where cross-section classification is generally determined based on the first order stress distribution. In reality, due to second order effects, the distribution of stresses is modified under increased loading; were the more favourable (due to the increased bending component) second order distribution of stresses to be utilised in the calculation of the strain limits, slightly increased deformation capacities and hence resistance predictions would be achieved.

5.3. Members subjected to combined compression and bending

In this section, the accuracy of the proposed approach is assessed for the in-plane design of stainless steel beam-columns. The assessment was carried out on a total of 297 hollow section beam-columns considering both major and minor axis buckling, three member slenderness values ($\bar{\lambda}$ = 0.5, 1.0, 1.5), and three bending moment distributions along the member length (ψ = 1.0, 0, -0.5), achieved by changing the ratio of applied end moments $\psi = M_2/M_1$, where M_1 and M_2 are the applied end moments. The ratio of applied compression to bending was varied to cover the full range of loading scenarios from pure compression to pure bending.

Figures 10 to 12 show normalised M-N interaction diagrams for some example hollow section beam-columns subjected to combined compression and bending with ψ = 0, ψ = 1 and ψ = -0.5, respectively. In the figures, the resistance predictions obtained using the proposed design approach (i.e. beam element GMNIA + CSM strain limits) are compared with the shell benchmark FE capacities, as well as two alternative EN 1993-1-4 [8] design approaches: (i) utilising a second order elastic analysis (GNIA) with a linear interaction cross-section check, and (ii) traditional member buckling checks. Note that the member buckling checks were carried out utilising the revised interaction equations for hollow sections, based on the work carried out by Zhao et al. [48], included in the Fourth Edition of the Design Manual for Structural Stainless Steel [49] and expected to be included in the upcoming revision of EN 1993-1-4. In the classification of the cross-sections, the simplified definition of ε that is due to be included in the upcoming revision of EN 1993-1-4 [50], given by Eq. (16), was utilised.

$$\varepsilon = \sqrt{\frac{235}{f_y}} \tag{16}$$

The performed second order elastic analyses (GNIA) incorporated the equivalent bow imperfections included in prEN 1993-1-1 [44,46]; while Figures 10 and 12 present results for

Class 1 cross-sections and therefore utilise the equivalent bow imperfections for use with a linear plastic interaction M-N check, the cross-section presented in Figure 11 is Class 3 for the bending dominated cases and Class 4 in the compression dominated cases and therefore utilises the equivalent bow imperfections for use with a linear elastic interaction M-N check.

Good agreement can be seen between the proposed design approach and the benchmark FE results, while both EN 1993-1-4 design approaches result in significantly more conservative predictions, particularly in the bending dominated cases. This is emphasised in Figure 13, which shows the normalised radial resistance for the three considered design methods relative to the benchmark shell FE results, where the normalised radial resistance ε_{i}, where i signifies the design approach considered, is calculated using Eq. (17), where R_{FE} and R_{d} are the radial distances measured from the origin to the data point in M-N space determined from the benchmark shell FE model and the considered design approach, respectively – see Figure 14. Values of ε_{i} larger than unity indicate conservative strength predictions. Table 5 presents a summary of the normalised radial resistances, including the mean and COV values for each design method.

$$\varepsilon_{\mathrm{i}} = \frac{R_{\mathrm{FE}}}{R_{\mathrm{d}}} \tag{17}$$

Second order elastic analysis with a linear cross-section check results in more accurate resistance predictions than the member buckling checks, but the predictions are still overly conservative compared with the benchmark shell FE results, particularly in the bending dominated cases. While the effects of geometric imperfections and residual stresses are accounted for in the analysis through the equivalent bow imperfections, the beneficial effects of local moment gradients and strain hardening are ignored. The proposed approach is accurate and consistent with an overall mean normalised radial resistance ϵ_{prop} of 1.11 and COV of 0.061 compared with overall mean normalised radial resistances of 1.30 and 1.21 and COVs of 0.167

and 0.088 for the EN 1993-1-4 member buckling checks ($\epsilon_{\text{EC-trad}}$) and GNIA + cross-section checks ($\epsilon_{\text{EC-adv}}$), respectively.

Overall, the proposed method of design by beam element second order inelastic analysis with CSM strain limits is more accurate and consistent compared to EN 1993-1-4 design, particularly for bending dominated cases. The design approach captures the beneficial effects of moment gradients on both global and local buckling, as well as strain hardening, and eliminates the need for buckling checks, the determination of effective lengths and moment gradients factors and the calculation of effective section properties for Class 4 cross-sections.

6. RELIABILITY ANALYSIS

The reliability analysis of the proposed design approach is assessed in this section. In the Eurocodes, partial safety factors γ_{M1} are applied in order to ensure the required level of reliability; EN 1993-1-4 [8] gives a recommended value for the partial safety factor γ_{M1} of 1.1 for stainless steel. The required partial safety factor γ_{M1} for use in design by second order inelastic analysis with CSM strain limits is assessed herein using the first order reliability method (FORM) set out in EN 1990 [51] for each design case considered. A target reliability index β of 3.8, corresponding to an overall target failure probability of 10^{-6} per year over a 50 year design life, was assumed as recommended in EN 1990.

The values of the material overstrength $f_{\text{y,mean}}/f_{\text{y,nom}}$, where $f_{\text{y,mean}}$ is the mean yield stress and $f_{\text{y,nom}}$ is the nominal yield stress, and the corresponding coefficient of variation of the yield strength V_{fy} were taken as those specified in Afshan et al. [52], as presented in Tables 6 to 8. The COV of the cross-sectional area V_{A}, calculated according to the formulae detailed in [52] and the variability of the dimensional parameters provided in prEN 1993-1-1 [44], were taken as 0.022 and 0.027 for the I-sections and hollow sections, respectively, and the COV of the

Young's modulus V_E taken equal to 0.03 [44]. The mean correction factor b was determined based on averaging the ratios of the benchmark resistances obtained from the shell FE models r_e to the predicted resistances obtained from the proposed design method r_t, as given by Eq. (18) [45,53].

$$b = \frac{1}{n}\sum_{i=1}^{n}\frac{r_{\mathrm{e,i}}}{r_{\mathrm{t,i}}} \tag{18}$$

To accurately account for the varying dependency on the basic variables – yield stress f_y, cross-sectional area A and Young's modulus E – for each individual design case considered, the dependence of the resistance, presented as the exponent (c, d and e) to which each basic variable should be raised were calculated using Eqs. (19)–(21), following the procedures set out in [45,52], where $N_{1.05fy}$ is the buckling load calculated from a numerical analysis with the yield stress f_y multiplied by 1.05, $N_{1.05A}$ is the buckling load calculated from a numerical analysis with the cross-sectional area A multiplied by 1.05, $N_{1.05E}$ is the buckling load calculated from a numerical analysis with the Young's modulus E multiplied by 1.05 and N_{fy}, N_A and N_E represent the original buckling load with no alterations to the yield stress, cross-sectional area or Young's modulus. Note that in the calculation of $N_{1.05fy}$ that the ultimate stress f_u was also multiplied by 1.05 to prevent a reduction in the slope of the second-stage of the Ramberg-Osgood material model. Using these exponents, the combined coefficient of variation V_{rt} was calculated for each design case.

$$c = \frac{\ln\left(N_{1.05f_{\mathrm{y}}}/N_{f_{\mathrm{y}}}\right)}{\ln\left(1.05f_{\mathrm{y}}/f_y\right)} \tag{19}$$

$$d = \frac{\ln(N_{1.05A}/N_A)}{\ln(1.05A/A)} \tag{20}$$

$$e = \frac{\ln(N_{1.05E}/N_E)}{\ln(1.05E/E)} \tag{21}$$

As discussed in Walport et al. [45], while the use of the mean value of the Young's modulus E = 200000 N/mm^2 is suitable for the resistance functions set out in EN 1993-1-4 [8] due to the partial safety factors having been calibrated on the basis of this reference value, it is not suitable for use in design by second order inelastic analysis. Consider, for example, a very slender column – the resistance obtained from a second order inelastic analysis will be dominated by the Young's modulus and close to the Euler load; use of the mean value of Young's modulus will result approximately in a mean (i.e. fiftieth percentile), rather than the traditionally targeted characteristic (i.e. fifth percentile) resistance, to which a partial safety factor is applied to achieve the design value of the resistance. Use of the characteristic value of E (i.e. the fifth percentile) is therefore recommended, as employed herein, in design by second order inelastic analysis.

Tables 6 to 8 present a summary of the results of the reliability analysis carried out according to EN 1990 [51]; Table 6 presents the results for members subjected to bending, Table 7 presents the results for members subjected to compression and Table 8 presents the results for members subjected to combined compression and bending. The partial safety factor, as well as the mean correction factor b and the coefficient of variation of the predicted resistances relative to the benchmark shell FE resistances V_δ are presented for each case. For assessment of the proposed design approach for members subjected to bending, since there is an increasing level of conservatism for low and high cross-section slenderness, the test and FE data was grouped by cross-section slenderness ($\bar{\lambda}_p \leq 0.4$, $0.4 < \bar{\lambda}_p \leq 0.9$, $\bar{\lambda}_p > 0.9$); the values of b and V_δ were calculated for each group and these were used to calculate the overall partial safety factor γ_{M1}. Table 6 presents the mean values of b, V_δ and γ_{M1}.

It can be seen from Tables 6 to 8 that the mean predictions are safe sided, with all b values greater than unity, and that the required partial safety factors γ_{M1} for design by second order inelastic analysis with CSM strain limits are less than the recommended value of 1.1 for stainless steel. Therefore, the design method can be safely adopted in conjunction with this partial factor. Note that if the values of $f_{y,mean}/f_{y,nom}$ and V_{fy} are taken as 1.2 and 0.045 instead of 1.3 and 0.060 (as assumed in the reliability analyses performed in the development of AISC 370 [37]) that the calculated values of γ_{M1} still lie below the recommended value of γ_{M1} equal to 1.1 in all cases.

7. SUMMARY OF DESIGN PROPOSALS AND WORKED EXAMPLES

A summary of the design proposals made herein, and the steps involved in the application of the method are shown in Figure 15. Two worked examples are presented in this section to illustrate the application of the proposed design method of beam element second order inelastic analysis with CSM strain limits. Worked example 1 considers a duplex stainless steel RHS 200×100×5 member under three-point bending and worked example 2 considers an austenitic stainless steel HEB 140 I-section member subjected to combined major axis bending and compression. Note that centreline dimensions have been used in all the following calculations, with the effects of fillets and corner radii ignored.

7.1. Worked example 1

Worked example 1 considers an S450 Grade 1.4462 duplex stainless steel (f_y = 450 N/mm^2) RHS 200×100×5 simply-supported beam of 1.5 m span subjected to a centrally applied point load F_d = 230 kN, as shown in Figure 16. A stiffener at the point of the applied load prevents load failure under the concentrated transverse force. Following the design approach outlined in Figure 15, it is first necessary to calculate the full cross-section local buckling stress $\sigma_{cr,cs}$ [40] (step 1a) and the local buckling half-wavelength $L_{b,cs}$ [24] (step 1b). With these values, the corresponding cross-section slenderness $\bar{\lambda}_{\mathrm{p}}$ (step 1c) and CSM strain limit $\varepsilon_{\mathrm{csm}}$ (step 1d) values are calculated. A second order inelastic analysis with equivalent bow imperfections is then carried out under the design loading (steps 2 and 3). Finally, the CSM strain limit is evaluated against the averaged strains from the beam FE model at all cross-sections (steps 4 and 5), and the resistance verification under the applied loading is performed (step 6).

7.1.1. Step 1a: Calculation of full cross-section local buckling stress $\sigma_{\mathrm{cr,cs}}$

The expressions developed by Gardner et al. [40] are used in this section to calculate the full cross-section local buckling stress $\sigma_{\mathrm{cr,cs}}$. The plate buckling coefficients for the isolated internal flange under uniform compression with simply-supported $k_{\mathrm{f}}^{\mathrm{SS}}$ and fixed $k_{\mathrm{f}}^{\mathrm{F}}$ boundary conditions are $k_{\mathrm{f}}^{\mathrm{SS}}$=4.0 and $k_{\mathrm{f}}^{\mathrm{F}}$=6.97. For the internal web in bending, these are equal to $k_{\mathrm{w}}^{\mathrm{SS}}$=23.9 and $k_{\mathrm{w}}^{\mathrm{F}}$=39.6. The corresponding elastic buckling stresses are: $\sigma_{\mathrm{cr,f}}^{\mathrm{SS}} = 1913$ MPa, $\sigma_{\mathrm{cr,f}}^{\mathrm{F}} = 3333$ MPa, $\sigma_{\mathrm{cr,w}}^{\mathrm{SS}} = 2713$ MPa and $\sigma_{\mathrm{cr,w}}^{\mathrm{F}} = 4494$ MPa.

Since the maximum compressive stress in the flange and web are the same, the load correction factors β_{f} and β_{w} are equal to unity. The lower and upper bounds to the full cross-section local buckling stress are therefore:

$$\sigma_{\mathrm{cr,p}}^{\mathrm{SS}} = \min\left(\beta_{\mathrm{f}}\sigma_{\mathrm{cr,f}}^{\mathrm{SS}}, \beta_{w}\sigma_{\mathrm{cr,w}}^{\mathrm{SS}}\right) = 1913\ \mathrm{MPa}$$

$$\sigma_{\mathrm{cr,p}}^{\mathrm{F}} = \min\left(\beta_{\mathrm{f}}\sigma_{\mathrm{cr,f}}^{\mathrm{F}}, \beta_{w}\sigma_{\mathrm{cr,w}}^{\mathrm{F}}\right) = 3333\ \mathrm{MPa}$$

The interaction coefficient ζ, to account for the effects of element interaction, is given, for an I-section under major axis bending, by:

$$\zeta = (0.24 - a_{\mathrm{f}}\phi)^{0.6}$$

where $\phi = \sigma_{\mathrm{cr,f}}^{\mathrm{SS}}/\sigma_{\mathrm{cr,w}}^{\mathrm{SS}} = 0.70$ and $a_{\mathrm{f}} = 0.24 - \left[0.1\left(\frac{h}{b} - 1\right)\right]^{\frac{1}{0.6}}$ but $a_{\mathrm{f}} \leq 0.24$, hence $a_{\mathrm{f}} = 0.22$. Therefore, $\zeta = 0.23$, and the full cross-section local buckling stress $\sigma_{\mathrm{cr,cs}}$ is calculated

$$\sigma_{\mathrm{cr,cs}} = \sigma_{\mathrm{cr,p}}^{\mathrm{SS}} + \zeta\left(\sigma_{\mathrm{cr,p}}^{\mathrm{F}} - \sigma_{\mathrm{cr,p}}^{\mathrm{SS}}\right) = 1913 + 0.23(3333 - 1913) = 2240\ \mathrm{MPa}$$

Note that using the finite strip analysis software CUFSM [23] would give a full cross-section local buckling stress of 2328 MPa.

7.1.2. Step 1b: Calculation of local cross-section slenderness $\bar{\lambda}_{\mathrm{p}}$

The local cross-section slenderness $\bar{\lambda}_{\mathrm{p}}$ can be calculated using Eq. (5), and in the case of the critical cross-section:

$$\bar{\lambda}_{\mathrm{p}} = \sqrt{\frac{f_{\mathrm{y}}}{\sigma_{\mathrm{cr,cs}}}} = \sqrt{\frac{450}{2240}} = 0.45$$

7.1.3. Step 1c: Calculation of CSM strain limit $\varepsilon_{\mathrm{csm}}$

Based on the cross-section slenderness, the CSM strain limit may be calculated using Eqs. (3) and (4). For the critical cross-section, where $\bar{\lambda}_{\mathrm{p}}$=0.45, the CSM strain limit $\varepsilon_{\mathrm{csm}}/\varepsilon_{\mathrm{y}}$ is given by:

$$\frac{\varepsilon_{\mathrm{csm}}}{\varepsilon_{\mathrm{y}}} = \frac{0.25}{\bar{\lambda}_{\mathrm{p}}^{3.6}} + \frac{0.002}{\varepsilon_{\mathrm{y}}} = \frac{0.25}{0.45^{3.6}} + \frac{0.002}{450/191000} = 5.28$$

7.1.4. Step 1d: Calculation of local buckling half-wavelength $L_{\mathrm{b,cs}}$

The expressions developed by Fieber et al. [24] are used in this section to calculate the local buckling half-wavelength based on the full cross-section local buckling stress calculated in Section 7.1.1.

The lower and upper bound local buckling half-wavelengths are given by $L_{\mathrm{b,p}}^{\mathrm{F}}$ = 70 mm and $L_{\mathrm{b,p}}^{\mathrm{SS}}$ = 104 mm.

Finally, the local buckling half-wavelength is given by

$$L_{\mathrm{b,cs}} = L_{\mathrm{b,p}}^{\mathrm{SS}} - \zeta\left(L_{\mathrm{b,p}}^{\mathrm{SS}} - L_{\mathrm{b,p}}^{\mathrm{F}}\right) = 104 - 0.23(104 - 70) = 96\ \mathrm{mm}$$

Note that using the finite strip analysis software CUFSM [23] would give a local buckling half-wavelength of 98 mm.

7.1.5. Steps 2 and 3: Beam FE analysis

In this design example, a member length L of 1500 mm is considered with 64 elements used to discretise the member length and, therefore, four whole elements lie within the local buckling half-wavelength ($L_{b,cs}/(L/64)$ = 96/(1500/64) = 4.10). The material properties for S450 Grade 1.4462 duplex stainless steel were taken as f_y = 450 N/mm^2, f_u = 650 N/mm^2, and n = 8, as obtained from prEN 1993-1-4 [50], and m = 2.94 and ε_u = 0.31, as calculated using the expression in prEN 1993-1-14 [14,41], with the characteristic value of E = 191000 N/mm^2, and were employed through the two-stage Ramberg-Osgood material model. Figure 17 shows the response of the member from the second order inelastic Riks [11] analysis.

7.1.6. Steps 4 and 5: Verification against CSM strain limits

Cross-section resistance is verified by applying the CSM strain limit to the outer fibre compressive strains output from the beam FE analysis. By employed strain averaging, the beneficial effects of moment gradients are captured. As outlined in Section 7.1.5, in this example, four whole elements lie within the local buckling half-wavelength. The beam is under three-point bending and therefore the location of the critical cross-section is at the centre of the beam; the presence of the stiffener locally constrains the shape of the cross-section and hence the local buckling half-wavelength is located to either side of the stiffener. The characteristic resistance of the member (i.e. F_{Rk}) is equal to the load at which the average strain over this local buckling half-wavelength reaches the CSM strain limit.

7.1.7. Step 6: Resistance verification against applied loading

Since there is no peak load in the analysed simply-supported beam, the load level at which the average strain over the local buckling half-wavelength for each cross-section first reaches the

CSM strain limit denotes the characteristic value of the resistance of the member. It is necessary to apply the partial safety factor to get the design resistance, as given by Eq. (10). In this worked example, the CSM strain limit is reached at a load factor of 1.12 (F_{Rk} = 258 kN). Hence, the design resistance F_{Rd} is given by:

$$F_{\mathrm{Rd}} = \frac{F_{\mathrm{Rk}}}{\gamma_{\mathrm{M1}}} = \frac{258}{1.1} = 235\ \mathrm{kN}$$

And

$$\frac{F_{\mathrm{d}}}{F_{\mathrm{Rd}}} = \frac{230}{235} = 0.98 \leq 1.0 \quad \therefore\ \text{Pass}$$

Note that if an EN 1993-1-4 [8] cross-section check, where the cross-section is limited to the plastic moment capacity M_{pl}, is applied and used to calculated the resistance of member, the member would fail.

7.2. Worked example 2

Worked example 2 considers an S210 Grade 1.4301 austenitic (f_y=210 N/mm^2) stainless steel HEB 140 I-section member with a length L = 5600 mm subjected to the design loading F_d resulting in a major axis bending moment $M_{y,Ed}$ = 52.4 kNm and axial compression N_{Ed} =48.2 kN , as shown in Figure 18. Following the design approach outlined in Figure 15, it is first necessary to calculate the full cross-section local buckling stress $\sigma_{cr,cs}$ [40] (step 1a) and the local buckling half-wavelength $L_{b,cs}$ [24] (step 1b). As discussed in Section 5.2, these are calculated based on the first order stress distribution. Note that these parameters vary along the member length with the changing stress distribution; for simplicity the results presented below are for the critical cross-section only. With these values, the corresponding cross-section slenderness $\bar{\lambda}_{\mathrm{p}}$ (step 1c) and CSM strain limit $\varepsilon_{\mathrm{csm}}$ (step 1d) values are calculated. A second order inelastic analysis with equivalent bow imperfections is then carried out under the design loading (steps 2 and 3). Finally, the averaged strains from the beam FE model are evaluated against the CSM strain limits at all cross-sections (steps 4 and 5), and the applied loading is assessed against the calculated resistance (step 6).

7.2.1. Step 1a: Calculation of full cross-section local buckling stress $\sigma_{cr,cs}$

The expressions developed by Gardner et al. [40] are used in this section to calculate the full cross-section local buckling stress $\sigma_{cr,cs}$. The plate buckling coefficients for the isolated outstand flange under uniform compression with simply-supported $k_{\mathrm{f}}^{\mathrm{SS}}$ and fixed $k_{\mathrm{f}}^{\mathrm{F}}$ boundary conditions are $k_{\mathrm{f}}^{\mathrm{SS}}$=0.43 and $k_{\mathrm{f}}^{\mathrm{F}}$=1.25. For the internal web under combined compression and major axis bending, these are equal to $k_{\mathrm{w}}^{\mathrm{SS}}$=21.47 and $k_{\mathrm{w}}^{\mathrm{F}}$=35.82. The corresponding elastic buckling stresses are: $\sigma_{\mathrm{cr,f}}^{\mathrm{SS}}$ = 2181 MPa, $\sigma_{\mathrm{cr,f}}^{\mathrm{F}}$ = 6341 MPa, $\sigma_{\mathrm{cr,w}}^{\mathrm{SS}}$ = 11088 MPa and $\sigma_{\mathrm{cr,w}}^{\mathrm{F}}$ = 18496 MPa.

Since the maximum compressive stress in the flange and web are the same, the load correction factors β_{f} and β_{w} are equal to unity. The lower and upper bounds to the full cross-section local buckling stress are therefore:

$$\sigma_{\mathrm{cr,p}}^{\mathrm{SS}} = \min\left(\beta_{\mathrm{f}}\sigma_{\mathrm{cr,f}}^{\mathrm{SS}}, \beta_{w}\sigma_{\mathrm{cr,w}}^{\mathrm{SS}}\right) = 2181 \text{ MPa}$$

$$\sigma_{\mathrm{cr,p}}^{\mathrm{F}} = \min\left(\beta_{\mathrm{f}}\sigma_{\mathrm{cr,f}}^{\mathrm{F}}, \beta_{w}\sigma_{\mathrm{cr,w}}^{\mathrm{F}}\right) = 6341 \text{ MPa}$$

The interaction coefficient ζ, to account for the effects of element interaction, is given, for an I-section under major axis bending, by:

$$\zeta = 0.15\frac{t_{\mathrm{f}}}{t_{\mathrm{w}}}\phi \quad \text{but} \quad \zeta \geq \frac{t_{\mathrm{w}}}{t_{\mathrm{f}}}(0.4 - 0.25\phi)$$

where $\phi = \sigma_{\mathrm{cr,f}}^{\mathrm{SS}}/\sigma_{\mathrm{cr,w}}^{\mathrm{SS}} = 0.197$. Therefore, ζ = 0.205, and the full cross-section local buckling stress $\sigma_{cr,cs}$ is calculated as:

$$\sigma_{\mathrm{cr,cs}} = \sigma_{\mathrm{cr,p}}^{\mathrm{SS}} + \zeta\left(\sigma_{\mathrm{cr,p}}^{\mathrm{F}} - \sigma_{\mathrm{cr,p}}^{\mathrm{SS}}\right) = 2181 + 0.205(6341 - 2181) = 3034\ \mathrm{MPa}$$

Note that using the finite strip analysis software CUFSM [23] would give a full cross-section local buckling stress of 3096 MPa.

7.2.2. Step 1b: Calculation of local cross-section slenderness $\bar{\lambda}_{\mathrm{p}}$

The local cross-section slenderness $\bar{\lambda}_{\mathrm{p}}$ can be calculated using Eq. (5), and in the case of the critical cross-section:

$$\bar{\lambda}_{\mathrm{p}} = \sqrt{\frac{f_{\mathrm{y}}}{\sigma_{\mathrm{cr,cs}}}} = \sqrt{\frac{210}{3034}} = 0.26$$

7.2.3. Step 1c: Calculation of CSM strain limit $\varepsilon_{\mathrm{csm}}$

Based on the cross-section slenderness, the CSM strain limit may be calculated using Eqs. (3) and (4). For the critical cross-section, where $\bar{\lambda}_{\mathrm{p}}$ = 0.26, the CSM strain limit $\varepsilon_{\mathrm{csm}}/\varepsilon_{\mathrm{y}}$ is given by:

$$\frac{\varepsilon_{\mathrm{csm}}}{\varepsilon_{\mathrm{y}}} = \frac{0.25}{\bar{\lambda}_{\mathrm{p}}^{3.6}} + \frac{0.002}{\varepsilon_{\mathrm{y}}} = \frac{0.25}{0.26^{3.6}} + \frac{0.002}{210/191000} = 33.7$$

However, the CSM strain limit $\varepsilon_{\mathrm{csm}}/\varepsilon_{\mathrm{y}}$ is limited to 15 (Ω=15) and therefore, $\varepsilon_{\mathrm{csm}}/\varepsilon_{\mathrm{y}}$ = 15.

7.2.4. Step 1d: Calculation of local buckling half-wavelength $L_{\mathrm{b,cs}}$

The expressions developed by Fieber et al. [24] are used in this section to calculate the local buckling half-wavelength based on the full cross-section local buckling stress calculated in Section 7.2.1.

The lower and upper bound local buckling half-wavelengths are given by $L_{\mathrm{b,p}}^{\mathrm{F}}$ = 116 mm and $L_{\mathrm{b,p}}^{\mathrm{SS}}$ = 268 mm.

Finally, the local buckling half-wavelength is given by

$$L_{\mathrm{b,cs}} = L_{\mathrm{b,p}}^{\mathrm{SS}} - \zeta\left(L_{\mathrm{b,p}}^{\mathrm{SS}} - L_{\mathrm{b,p}}^{\mathrm{F}}\right) = 268 - 0.205(268 - 116) = 237\ \mathrm{mm}$$

Note that using the finite strip analysis software CUFSM [23] would give a local buckling half-wavelength of 250 mm.

7.2.5. Steps 2 and 3: Beam FE analysis

In this design example, the member length is 5600 mm, which corresponds to a member slenderness $\bar{\lambda}$ equal to 1.00. 72 elements were used to discretise the member length and, therefore, for the critical cross-section, three whole elements lie within the local buckling half-wavelength ($L_{\mathrm{b,cs}}/(L/72) = 237/(5600/72) = 3.05$). An equivalent bow imperfection in the shape of a half-sine wave and with a magnitude equal to $e_0 = \alpha L/150$ (but $\leq L/1000$) = 18.3 mm was modelled. The material properties for S210 Grade 1.4301 austenitic stainless steel were taken as f_y = 210 N/mm^2, f_u = 500 N/mm^2, and n = 7, as obtained from prEN 1993-1-4 [50], and m = 2.18 and ε_u = 0.58, as calculated using the expression in prEN 1993-1-14 [14,41], with the characteristic value of E = 191000 N/mm^2, were employed through the two-stage Ramberg-Osgood material model. Figure 19 shows the response of the member from the second order inelastic Riks [11] analysis.

7.2.6. Steps 4 and 5: Verification against CSM strain limits

Cross-section resistance is verified by applying the CSM strain limit to the outer fibre compressive strains output from the beam FE analysis. By employed strain averaging, the beneficial effects of moment gradients are captured. As outlined in Section 7.2.5, in this example, three whole elements lie within the local buckling half-wavelength. While in this design case, the analysis does exhibit a peak load, the CSM strain limit is reached at a lower load level and therefore governs. The element that reaches the CSM strain limit first defines the critical cross-section and the characteristic resistance of the member (i.e. F_{Rk}); in this example, the critical element is at the top end of the member (see Figure 19).

7.2.7. Step 6: Resistance verification against applied loading

The load level at which the first cross-section reaches the CSM strain limit gives the characteristic value of the resistance of the structure. It is necessary to apply the partial safety factor to obtain the design resistance, as given by Eq. (10). In this worked example, the CSM strain limit is reached at a load factor α of 1.15 i.e. F_{Rk}/F_d = 1.15.

$$F_{\mathrm{Rd}} = \frac{F_{\mathrm{Rk}}}{\gamma_{\mathrm{M1}}}$$

Hence

$$\frac{F_{\mathrm{d}}}{F_{\mathrm{Rd}}} = \frac{1}{1.15/1.1} = 0.96 \ \leq 1.0 \quad \therefore \ \text{Pass}$$

Note that if the resistance of the member was calculated using an EN 1993-1-4 linear plastic cross-section check applied to the results of a second order plastic analysis with corresponding equivalent imperfections [47], the member would fail.

8. CONCLUSIONS

Beam finite elements are commonly used in advanced structural frame analysis for their computational efficiency but they are unable to capture the effects of local buckling. The development of a new method of structural stainless steel design by second order inelastic analysis where local buckling is simulated through the application of CSM strain limits has been presented. Design by advanced analysis is particularly appropriate for stainless steel structures due to the high material value and the complexities presented by the nonlinear material stress–strain response for traditional design treatments. Comparisons against current design methods confirm the consistent and significant benefits of the proposed method. A reliability analysis was conducted following EN 1990 with the derived partial safety factors below the target value of 1.1 in all cases confirming the safety of the design approach. The proposed method is due to be incorporated into the two major international stainless steel design standards – EN 1993-1-4 and AISC 370.

ACKNOWLEDGEMENTS

Funding for this investigation was received from the Imperial College PhD Scholarship scheme and the Engineering and Physical Sciences Research Council (EPSRC).

REFERENCES

[1] Trahair, N.S. 2018. Trends in the Code Design of Steel Framed Structures. *Advanced Steel Construction*, 14: 37–56.

[2] Walport, F., Gardner, L., & Nethercot, D.A. 2019. A method for the treatment of second order effects in plastically-designed steel frames. *Engineering Structures*, 200: 109516.

[3] Fieber, A., Gardner, L., & Macorini, L. 2019. Design of structural steel members by advanced inelastic analysis with strain limits. *Engineering Structures*, 199: 109624.

[4] Gardner, L., Yun, X., Fieber, A., & Macorini, L. 2019. Steel design by advanced analysis: material modeling and strain limits. *Engineering*, 5: 243–9.

[5] Fieber, A., Gardner, L., & Macorini, L. 2020. Structural steel design using second-order inelastic analysis with strain limits. *Journal of Constructional Steel Research*, 168: 105980.

[6] Thai, H.T., Uy, B., & Khan, M. 2015. A modified stress-strain model accounting for the local buckling of thin-walled stub columns under axial compression. *Journal of Constructional Steel Research*, 111: 57–69.

[7] Du, Z.L., Liu, Y.P., He, J.W., & Chan, S.L. 2019. Direct analysis method for noncompact and slender concrete-filled steel tube members. *Thin-Walled Structures*, 135: 173–84.

[8] EN 1993-1-4:2006 + A1: 2015. Eurocode 3 - Design of steel structures - Part 1-4: General rules - Supplementary rules for stainless steels. Brussels: CEN; 2015.

[9] EN 1993-1-1. 2005. Eurocode 3: Design of steel structures - Part 1-1: General rules and rules for buildings. Brussels: CEN; 2005.

[10] Walport, F., Gardner, L., Real, E., Arrayago, I., & Nethercot, D.A. 2019. Effects of material nonlinearity on the global analysis and stability of stainless steel frames. *Journal of Constructional Steel Research*, 152: 173–82.

[11] ABAQUS. 2014. Abaqus CAE User's Manual, Version 6.14. Pawtucket, USA: Hibbitt, Karlsson & Sorensen, Inc.; 2014.

[12] Mirambell, E., & Real, E. 2000. On the calculation of deflections in structural stainless steel beams: an experimental and numerical investigation. *Journal of Constructional Steel Research*, 54: 109–33.

[13] Rasmussen, K.J.R. 2003. Full-range stress–strain curves for stainless steel alloys. *Journal of Constructional Steel Research*, 59: 47–61.

[14] Arrayago, I., Real, E., & Gardner, L. 2015. Description of stress-strain curves for stainless steel alloys. *Materials and Design*, 87: 540–52.

[15] Gardner, L., & Yun, X. 2018. Description of stress-strain curves for cold-formed steels. *Construction and Building Materials*, 189: 527–38.

[16] ECCS. 1984. Ultimate limit state calculations of sway frames with rigid joints. *No 33, Technical Committee 8 of the European Convention for Constructional Steelwork (ECCS)*, 1984.

[17] Yuan, H.X., Wang, Y.Q., Shi, Y.J., & Gardner, L. 2014. Residual stress distributions in welded stainless steel sections. *Thin-Walled Structures*, 79: 38–51.

[18] Kucukler, M., Xing, Z., & Gardner, L. 2020. Behaviour and design of stainless steel I-section columns in fire. *Journal of Constructional Steel Research*, 164: 105890.

[19] Jandera, M., Gardner, L., & Machacek, J. 2008. Residual stresses in cold-rolled stainless steel hollow sections. *Journal of Constructional Steel Research,* 64: 1255–63.

[20] Gardner, L., & Nethercot, D.A. 2004. Numerical modeling of stainless steel structural components — A consistent approach. *Journal of Structural Engineering, ASCE,* 130: 1586–601.

[21] Ellobody, E., & Young, B. 2005. Structural performance of cold-formed high strength stainless steel columns. *Journal of Constructional Steel Research,* 61: 1631–49.

[22] EN 1993-1-5. 2009. Eurocode 3 - Design of steel structures - Part 1-5 : Plated structural elements. Brussels: CEN; 2009.

[23] Li, Z., & Schafer, B.W. 2010. Buckling analysis of cold-formed steel members with general boundary conditions using CUFSM: Conventional and constrained finite strip methods. *Proceedings Twentieth International Specialty Conference on Cold-Formed Steel Structures,*: 17–31.

[24] Fieber, A., Gardner, L., & Macorini, L. 2019. Formulae for determining elastic local buckling half-wavelengths of structural steel cross-sections. *Journal of Constructional Steel Research,* 159: 493–506.

[25] Bu, Y., & Gardner, L. 2018. Local stability of laser-welded stainless steel I-sections in bending. *Journal of Constructional Steel Research,* 148: 49–64.

[26] Theofanous, M., & Gardner, L. 2010. Experimental and numerical studies of lean duplex stainless steel beams. *Journal of Constructional Steel Research,* 66: 816–25.

[27] Afshan, S., & Gardner, L. 2013. Experimental study of cold-formed ferritic stainless steel hollow sections. *Journal of Structural Engineering ASCE,* 139: 717–28.

[28] Theofanous, M., & Gardner, L. 2009. Testing and numerical modelling of lean duplex

stainless steel hollow section columns. *Engineering Structures*, 31: 3047–58.

[29] Burgan, B.A., Baddoo, N.R., & Gilsenan, K.A. 2000. Structural design of stainless steel members — comparison between Eurocode 3, Part 1.4 and test results. *Journal of Constructional Steel Research*, 54: 51–73.

[30] Bu, Y., & Gardner, L. 2019. Laser-welded stainless steel I-section beam-columns: Testing, simulation and design. *Engineering Structures*, 179: 23–36.

[31] Zhao, O., Gardner, L., & Young, B. 2016. Buckling of ferritic stainless steel members under combined axial compression and bending. *Journal of Constructional Steel Research*, 117: 35–48.

[32] Cruise, R.B., & Gardner, L. 2008. Strength enhancements induced during cold forming of stainless steel sections. *Journal of Constructional Steel Research*, 64: 1310–6.

[33] Gardner, L. 2008. The continuous strength method. *Proceedings of the Institution of Civil Engineers - Structures and Buildings*, 161: 127–33.

[34] Afshan, S., & Gardner, L. 2013. The continuous strength method for structural stainless steel design. *Thin-Walled Structures*, 68: 42–9.

[35] Gardner, L., Wang, F., & Liew, A. 2011. Influence of strain hardening on the behavior and design of steel structures. *International Journal of Structural Stability and Dynamics*, 11: 855–75.

[36] Bock, M., Gardner, L., & Real, E. 2015. Material and local buckling response of ferritic stainless steel sections. *Thin-Walled Structures*, 89: 131–41.

[37] AISC. 2020. Draft Specification for Structural Stainless Steel Buildings, ANSI / AISC 370.

[38] Zhao, O., Afshan, S., & Gardner, L. 2017. Structural response and continuous strength

method design of slender stainless steel cross-sections. *Engineering Structures*, 140: 14–25.

[39] Zhang, X., Rasmussen, K.J.R., & Zhang, H. 2015. Structural modeling of cold-formed steel portal frames. *Structures*, 4: 58–68.

[40] Gardner, L., Fieber, A., & Macorini, L. 2019. Formulae for calculating elastic local buckling stresses of full structural cross-sections. *Structures*, 17: 2–20.

[41] prEN 1993-1-14. 2019. Eurocode 3 – Design of steel structures – Part 1-14: Design by FE analysis. *CEN*, Draft 1.

[42] Afshan, S., Zhao, O., & Gardner, L. 2019. Standardised material properties for numerical parametric studies of stainless steel structures and buckling curves for tubular columns. *Journal of Constructional Steel Research*, 152: 2–11.

[43] dos Santos, G.B., Gardner, L., & Kucukler, M. 2018. A method for the numerical derivation of plastic collapse loads. *Thin-Walled Structures*, 124: 258–77.

[44] prEN 1993-1-1. 2020. Eurocode 3 – Design of steel structures – Part 1-1: General rules and rules for buildings: 1–118.

[45] Walport, F., Gardner, L., & Nethercot, D.A. 2020. Equivalent bow imperfections for use in design by second order inelastic analysis. *Structures*, 26: 670–85.

[46] Lindner, J., Kuhlmann, U., & Jörg, F. 2018. Initial bow imperfections e0 for the verification of flexural buckling according to Eurocode 3 Part 1-1 – additional considerations. *Steel Construction*, 11: 30–41.

[47] Lindner, J., Kuhlmann, U., & Just, A. 2016. Verification of flexural buckling according to Eurocode 3 part 1-1 using bow imperfections. *Steel Construction*, 9: 349–62.

[48] Zhao, O., Gardner, L., & Young, B. 2016. Behaviour and design of stainless steel SHS

and RHS beam-columns. *Thin-Walled Structures*, 106: 330–45.

[49] SCI. 2017. Design Manual for Structural Stainless Steel Design. Fourth Edition. SCI Publication No. P413. UK: The Steel Construction Institute; 2017.

[50] prEN 1993-1-4. 2020. Eurocode 3 - Design of steel structures - Part 1-4: General rules - Supplementary rules for stainless steels. *CEN*, Draft 2.

[51] EN 1990. 2002. Eurocode - Basis of structural design. Brussels: CEN; 2002.

[52] Afshan, S., Francis, P., Baddoo, N.R., & Gardner, L. 2015. Reliability analysis of structural stainless steel design provisions. *Journal of Constructional Steel Research*, 114: 293–304.

[53] Meng, X., Gardner, L., Sadowski, A.J., & Rotter, J.M. 2020. Elasto-plastic behaviour and design of semi-compact circular hollow sections. *Thin-Walled Structures*, 148: 106486.

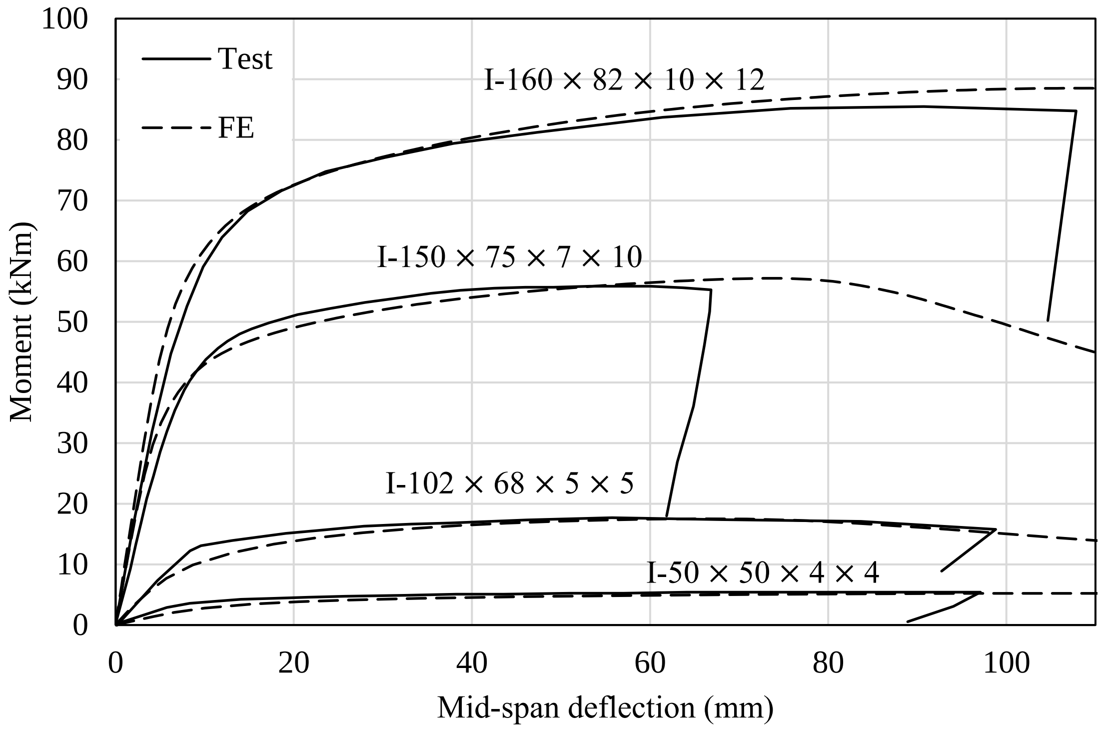

Figure 1: Shell FE model validation against a series of three-point bending tests on laser-welded austenitic stainless steel I-sections reported by Bu and Gardner [25].

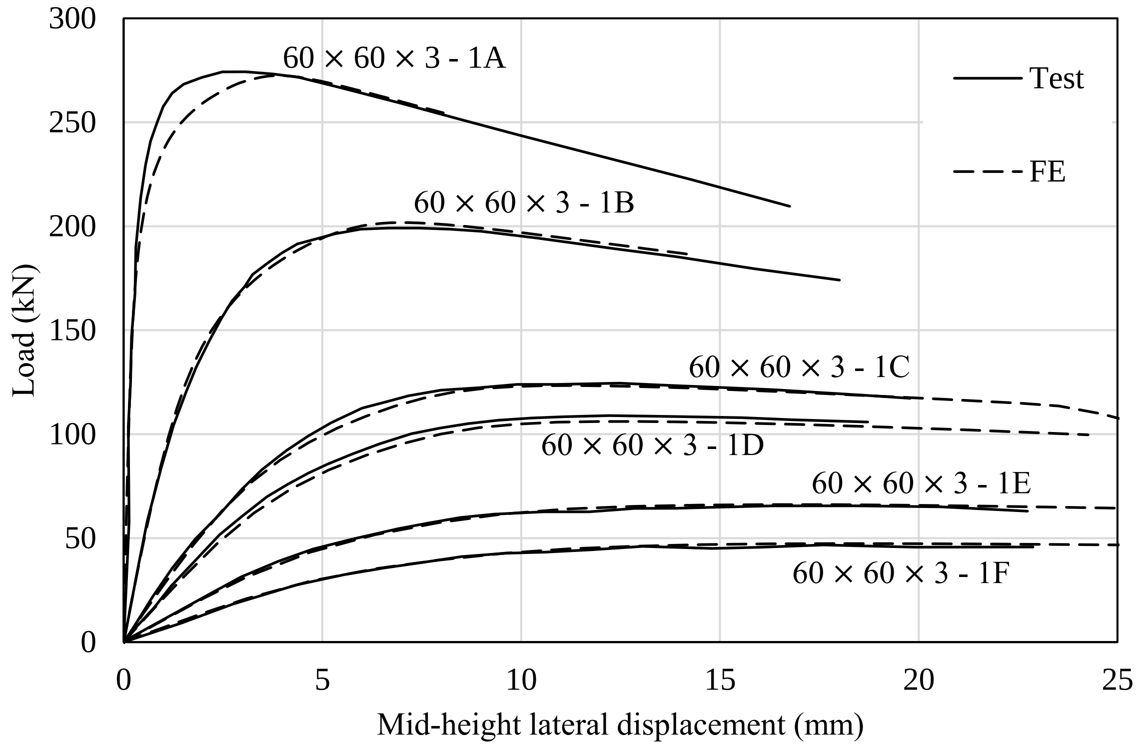

Figure 2: Shell FE model validation against a series of ferritic stainless steel SHS beam-column tests reported by Zhao et al. [31].

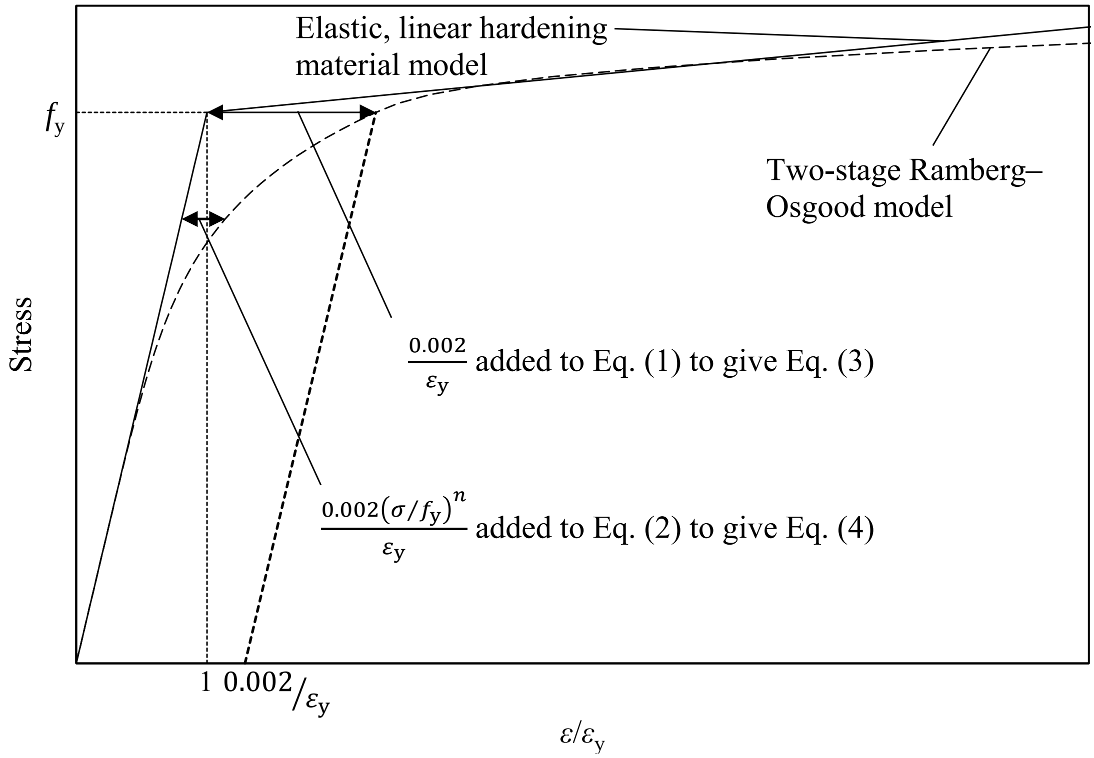

Figure 3: Illustration of modification of CSM base curves to reflect the use of different material models – an elastic, linear hardening material model for simplified hand calculations [34,35] and a compound Ramberg–Osgood material model for use in design by second order inelastic analysis, as proposed herein.

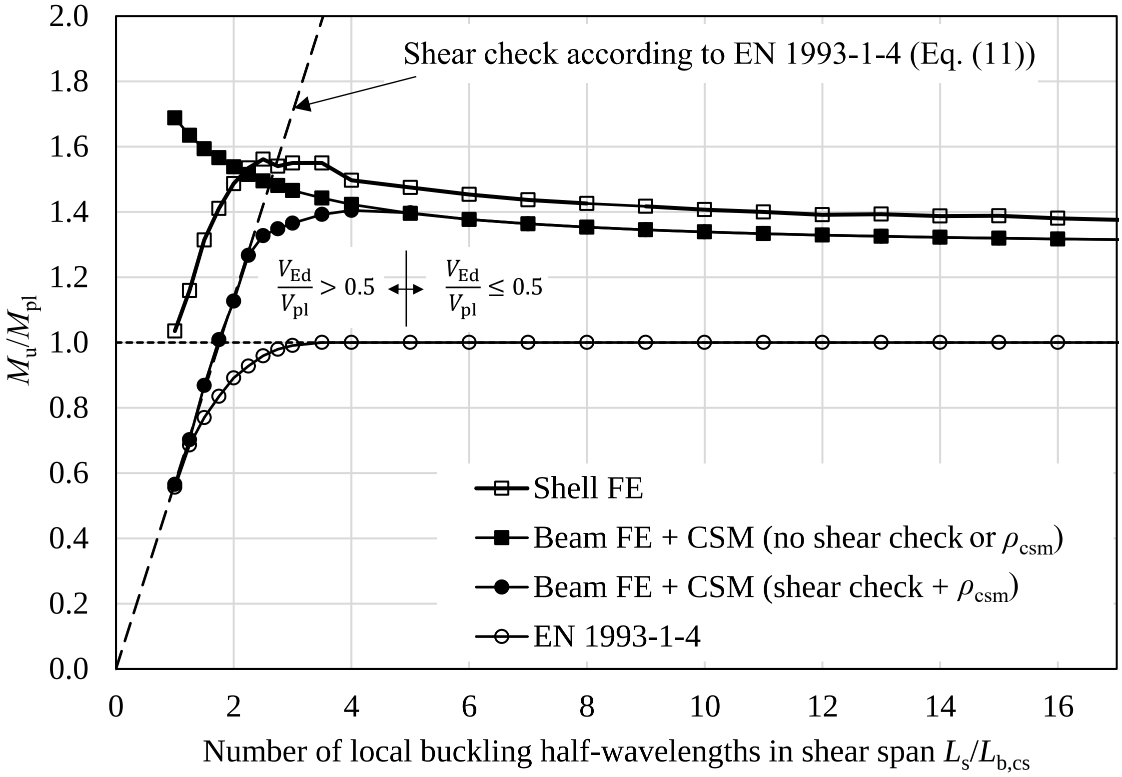

Figure 4: Effect of shear on the bending capacity of an austenitic stainless steel IPE 140 cross-section with varying member length under three-point bending.

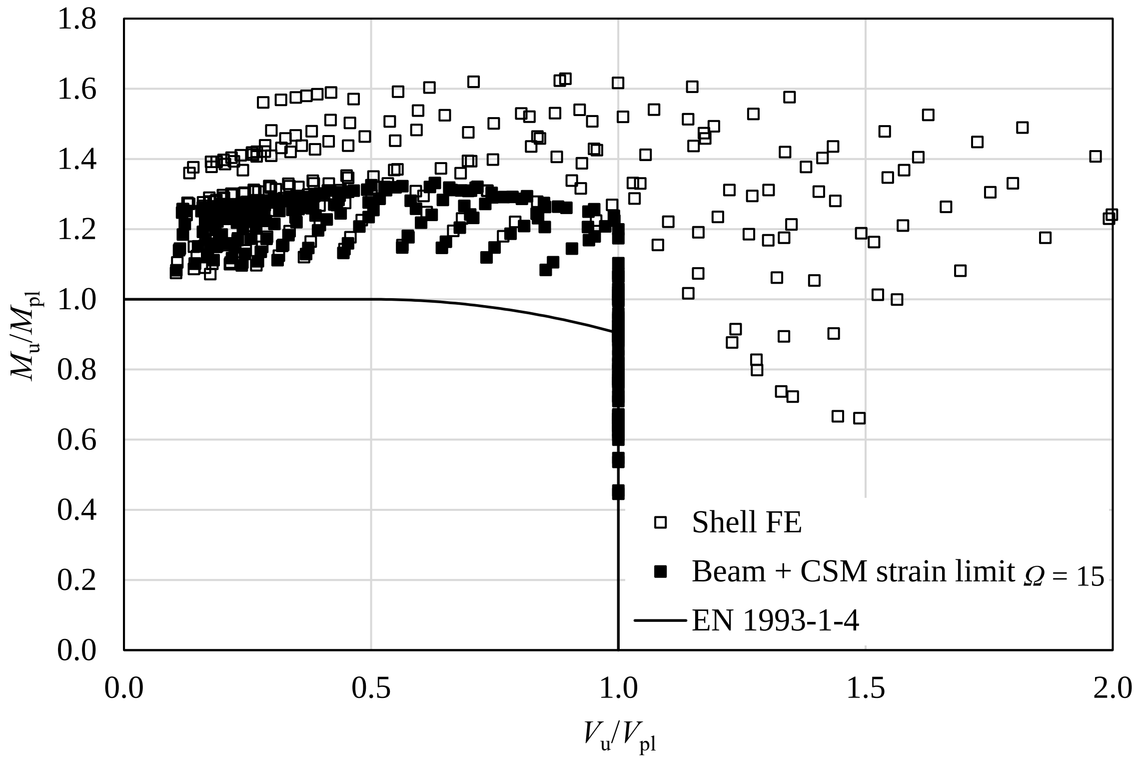

Figure 5: Moment-shear interaction for beams under three-point bending predicted by shell FE benchmark modelling, beam FE modelling with CSM strain limits and EN 1993-1-4 cross-section checks.

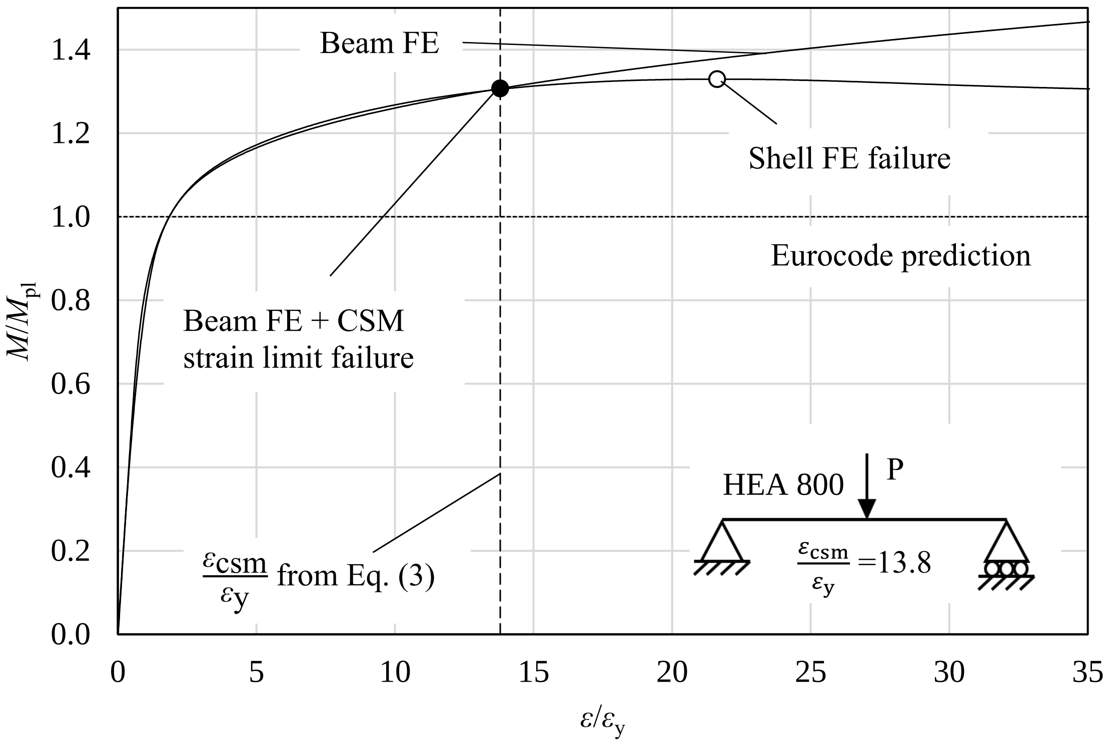

Figure 6: Response of an austenitic stainless steel HEA 800 simply-supported beam under three-point bending

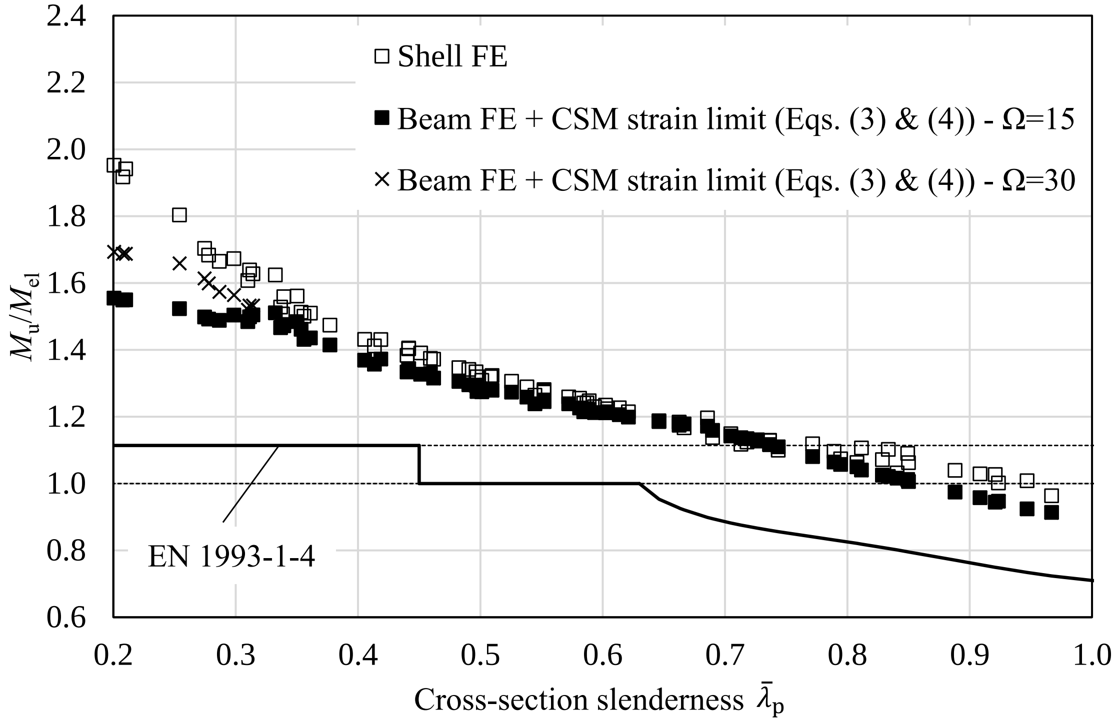

Figure 7: Capacity predictions for austenitic stainless steel I-sections of varying local slenderness subjected to three-point bending.

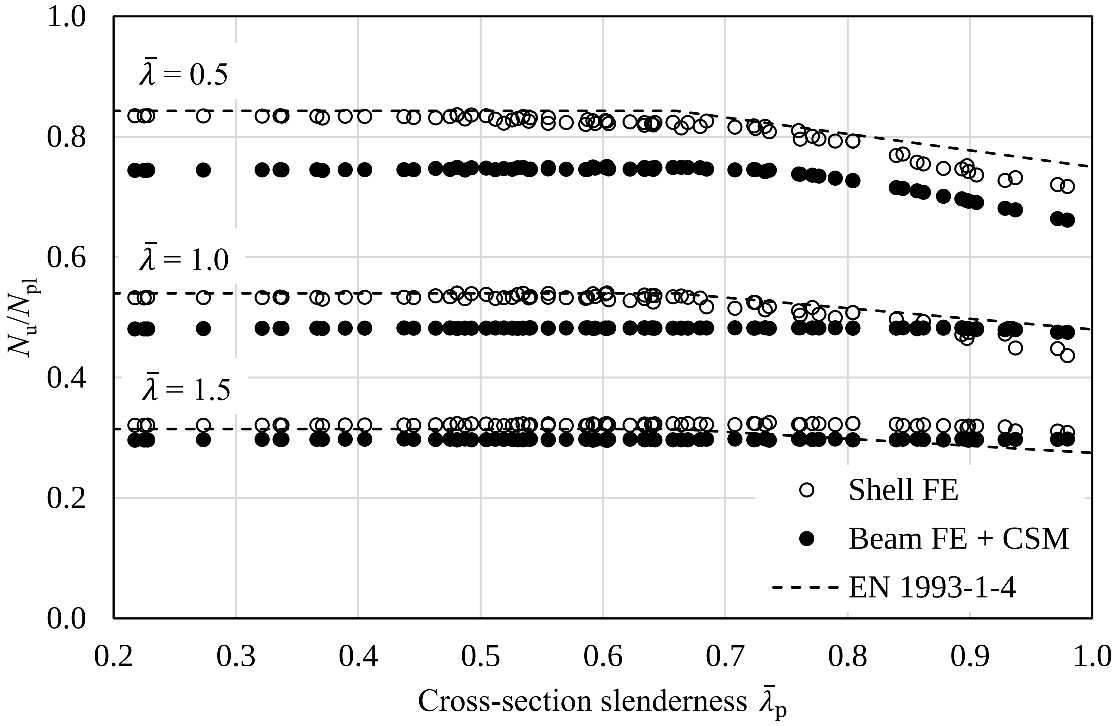

Figure 8: Resistance predictions of austenitic stainless steel I-section columns of varying cross-section slenderness $\bar{\lambda}_p$ buckling about the major axis for three values of member slenderness ($\bar{\lambda}$ = 0.5, 1.0, 1.5).

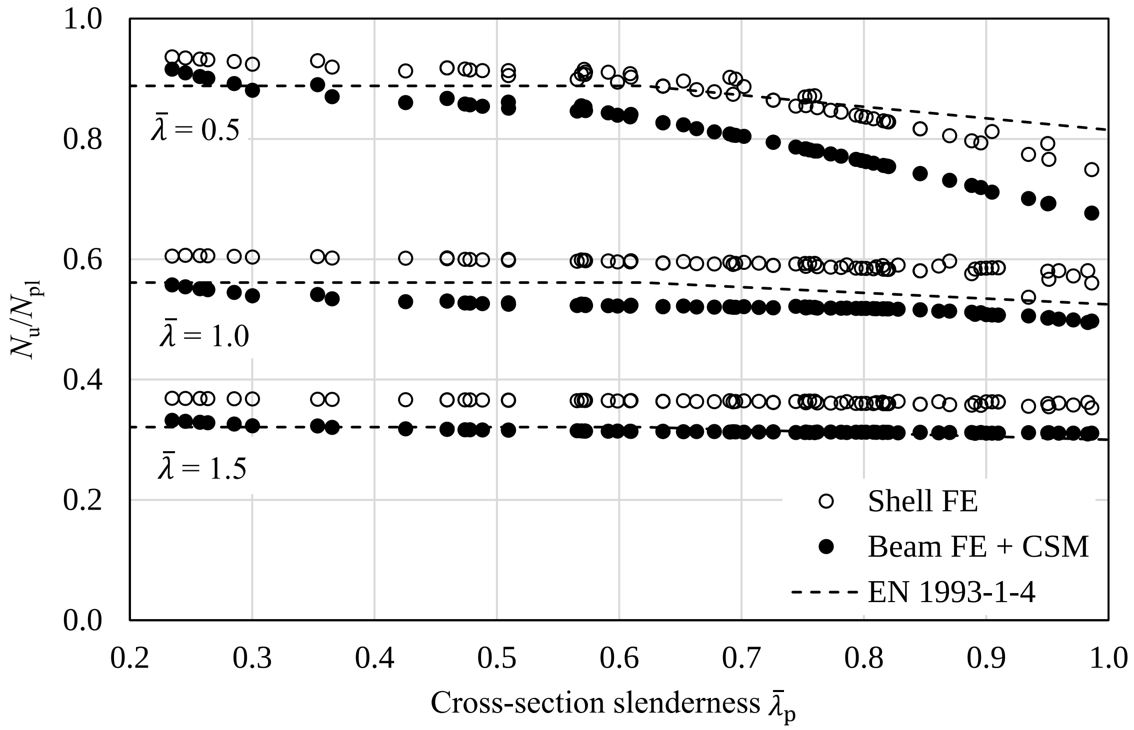

Figure 9: Resistance predictions of austenitic stainless steel hollow section columns of varying cross-section slenderness $\bar{\lambda}_p$ buckling about the major axis for three values of member slenderness ($\bar{\lambda}$ = 0.5, 1.0, 1.5).

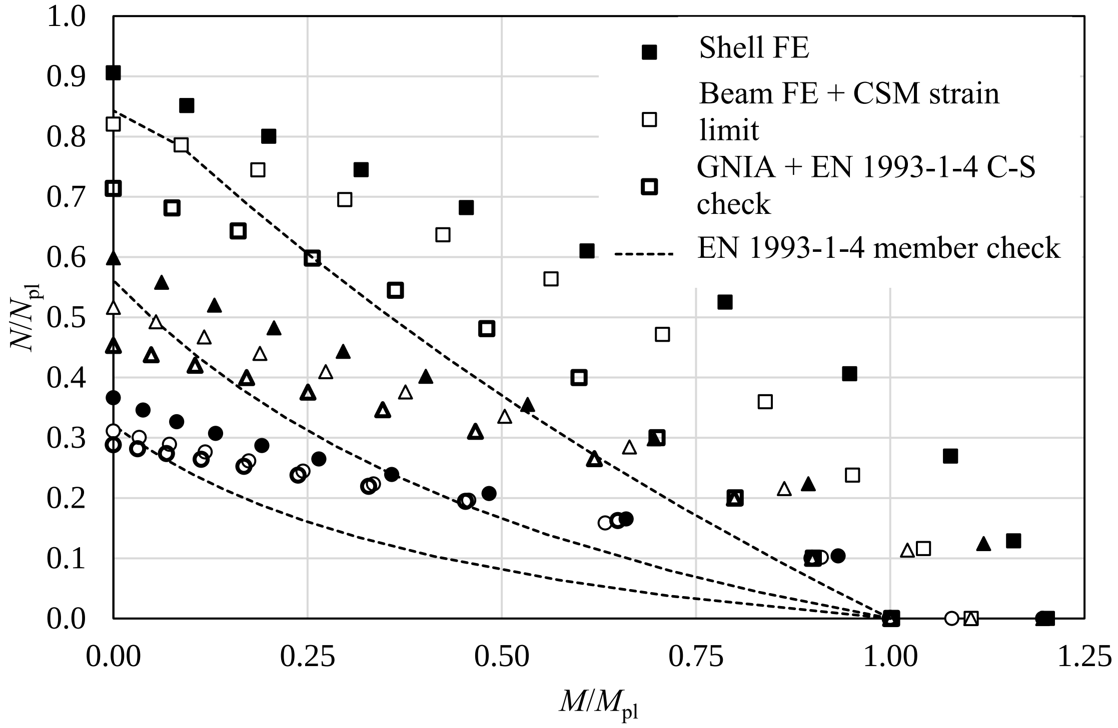

Figure 10: Normalised ultimate capacities of austenitic stainless steel SHS 100 × 100 × 4 pin-ended beam-columns buckling about the major axis with $\psi = 0$ considering three values of member slenderness ($\bar{\lambda}$ = 0.5 (squares), 1.0 (triangles), 1.5 (circles)).

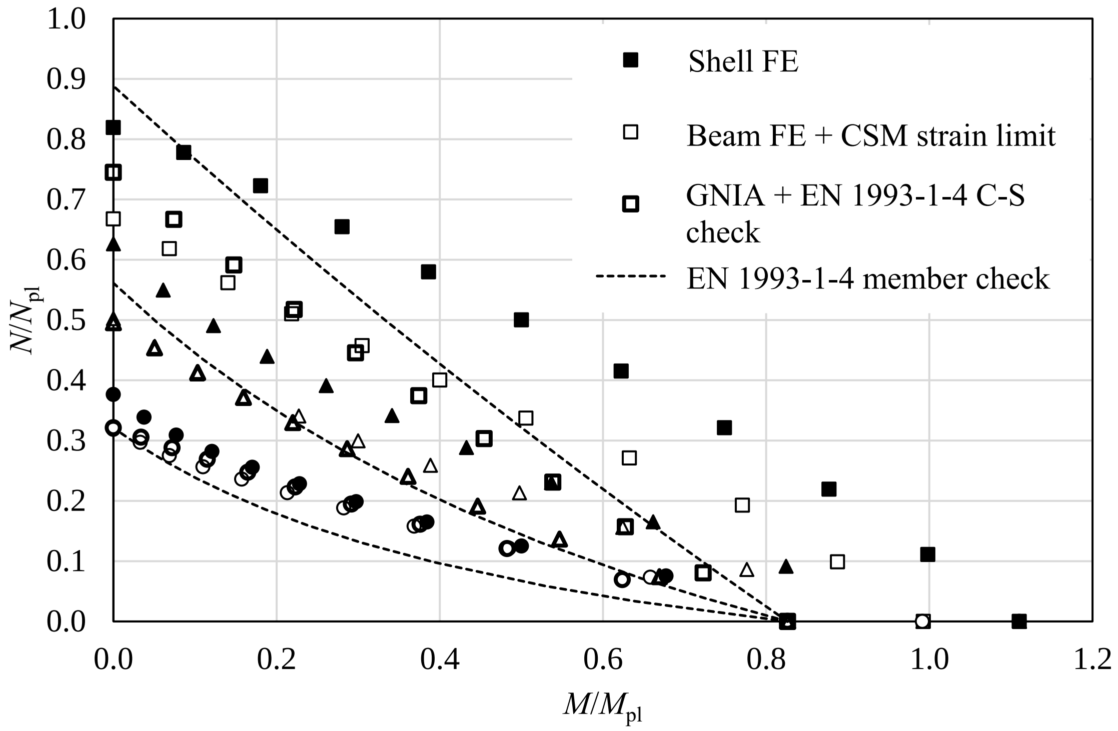

Figure 11: Normalised ultimate capacities of duplex stainless steel RHS 100 × 60 × 2.5 pin-ended beam-columns buckling about the major axis with ψ = 1 considering three values of member slenderness ($\bar{\lambda}$ = 0.5 (squares), 1.0 (triangles), 1.5 (circles)).

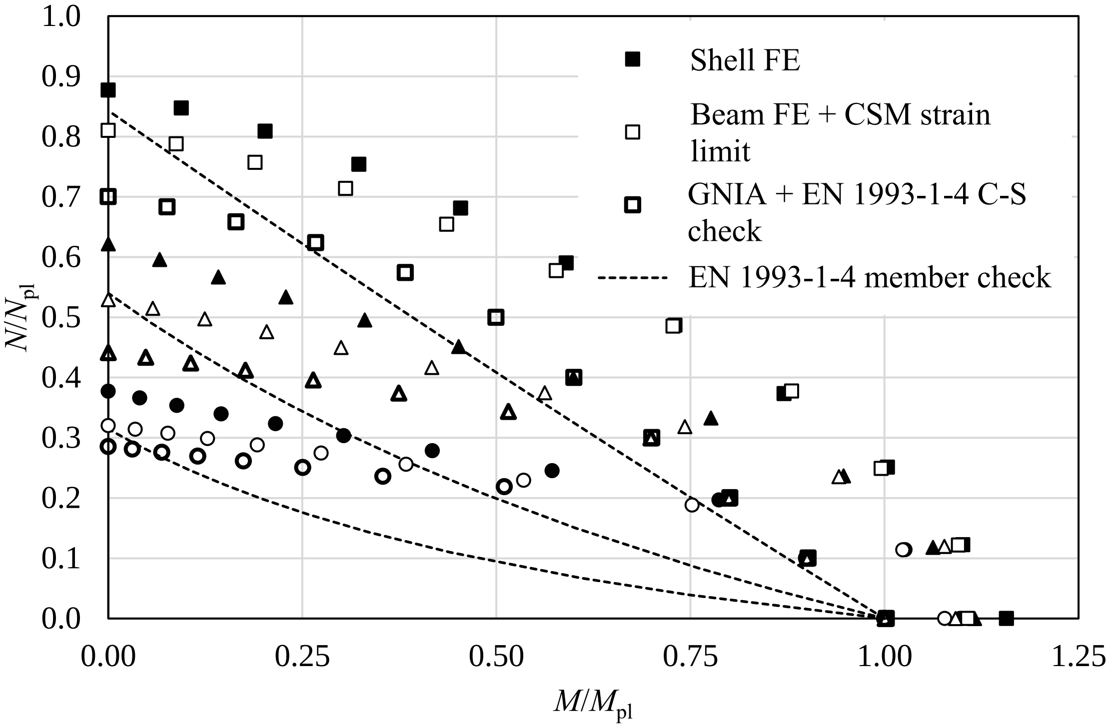

Figure 12: Normalised ultimate capacities of ferritic stainless steel RHS 120 × 60 × 5 pin-ended beam-columns buckling about the minor axis with ψ = -0.5 considering three values of member slenderness ($\bar{\lambda}$ = 0.5 (squares), 1.0 (triangles), 1.5 (circles)).

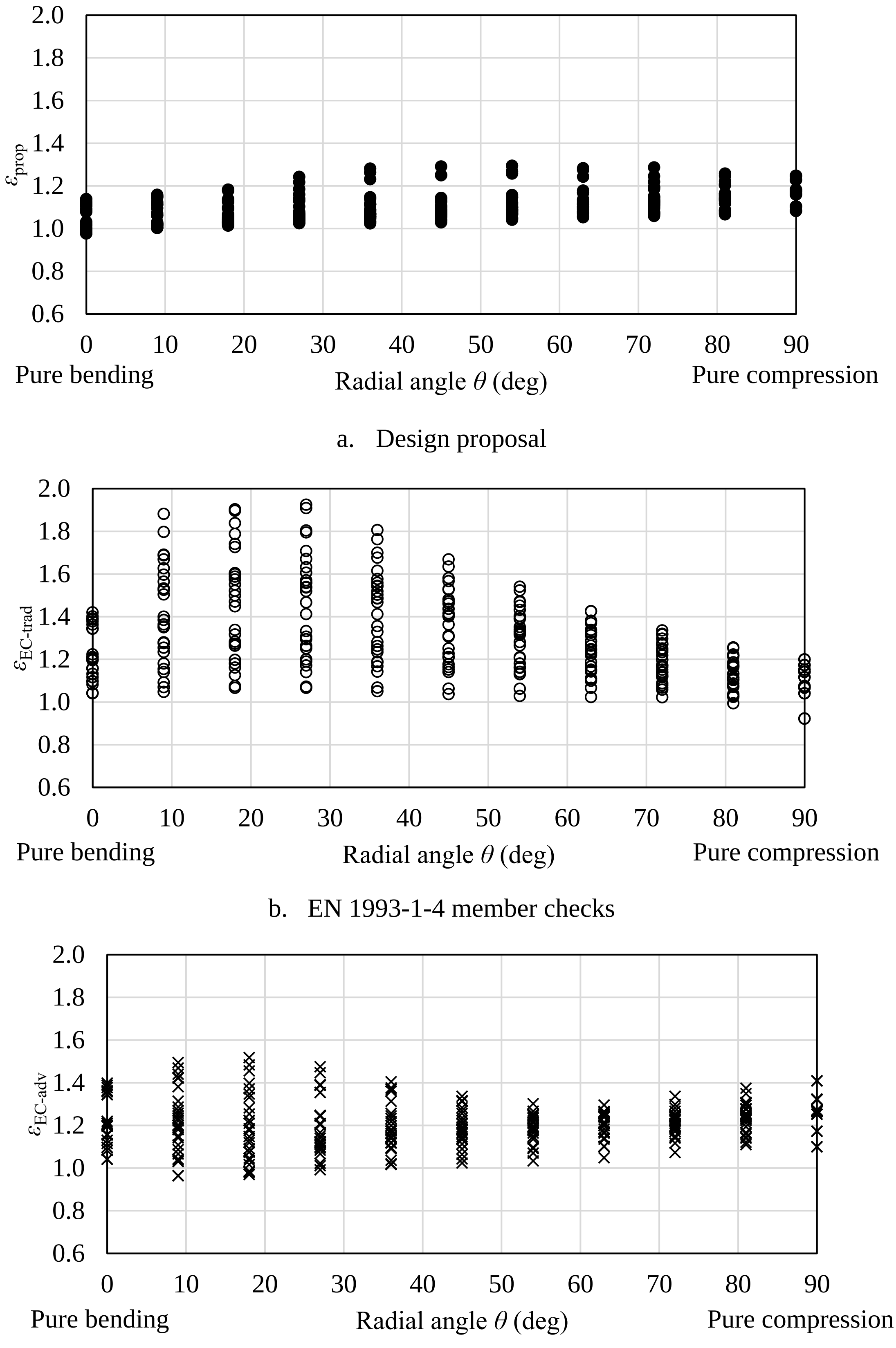

a. Design proposal

b. EN 1993-1-4 member checks

c. GNIA + EN 1993-1-4 C-S checks

Figure 13: Comparison of the resistance predictions obtained using the proposed design method and EN 1993-1-4 with the benchmark shell FE results.

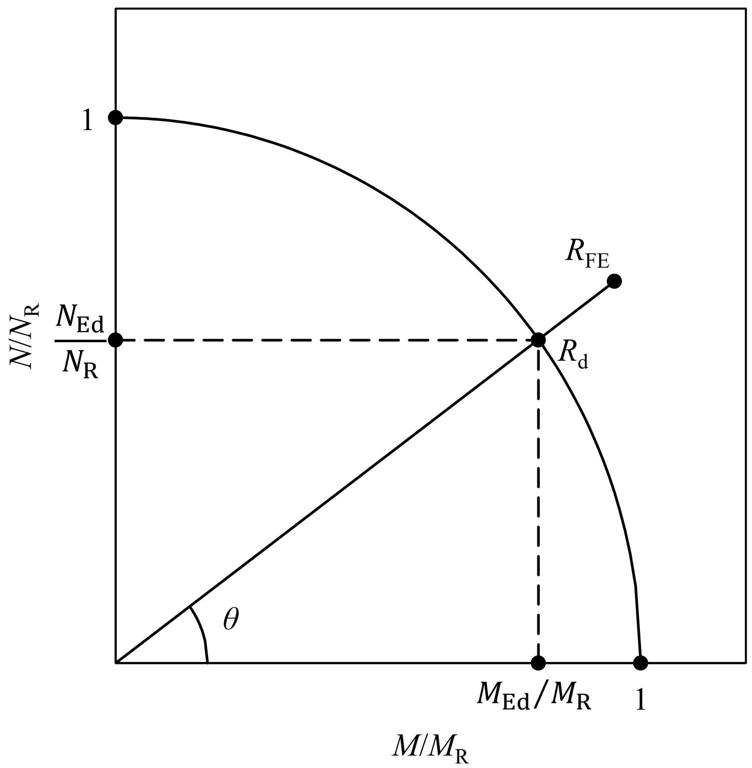

Figure 14: Definition of θ in normalised M-N interaction diagram.

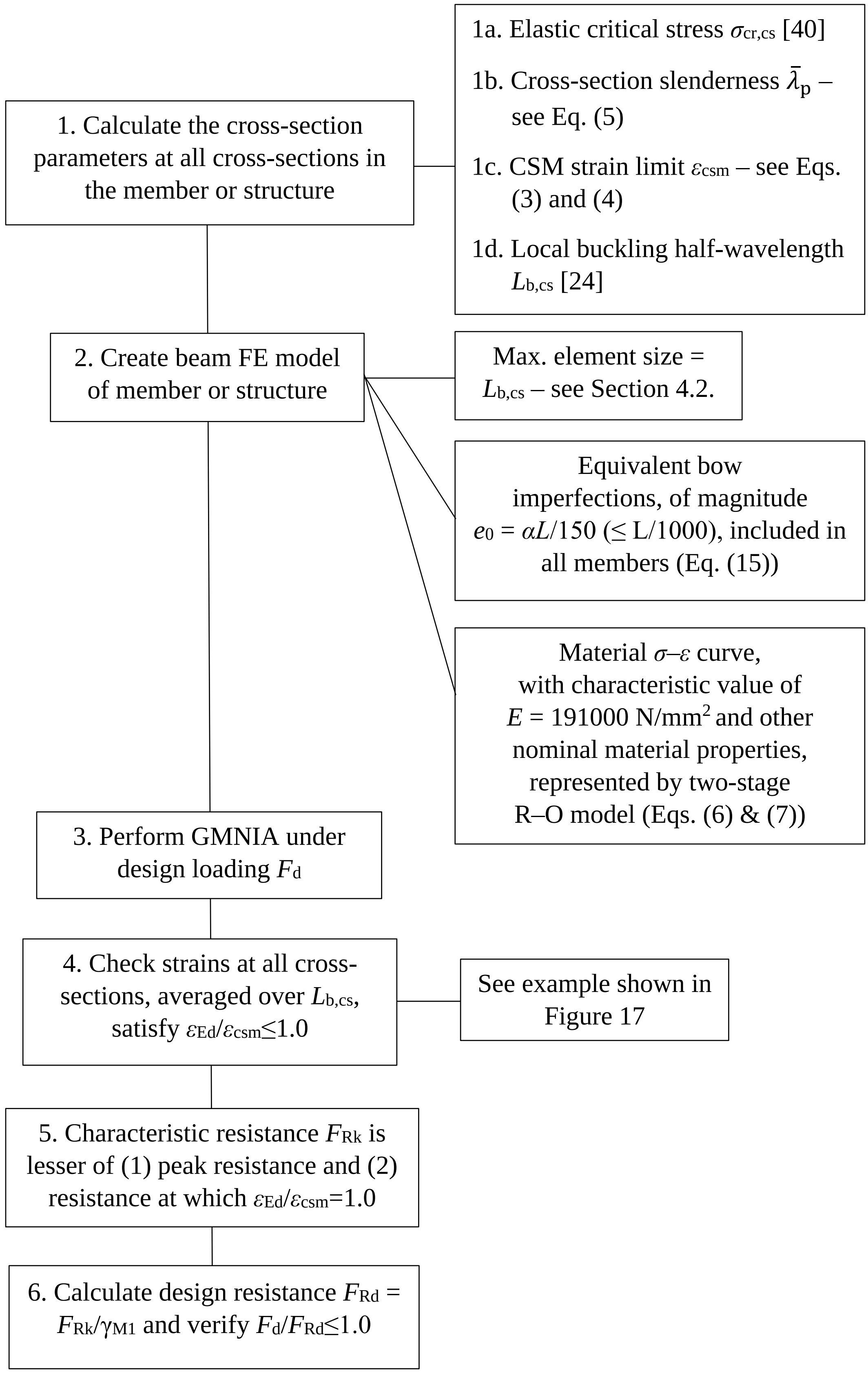

Figure 15: Steps involved in the application of the proposed design method.

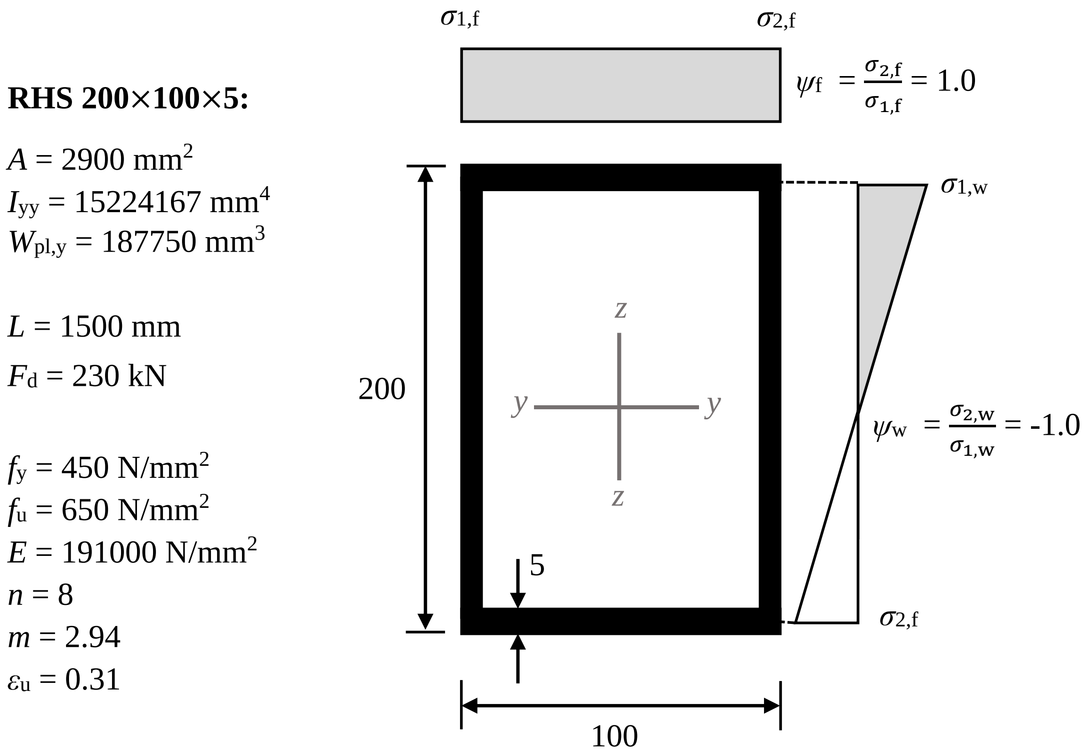

Figure 16: Worked example 1: RHS 200×100×5 cross-section subjected to major axis bending. All dimensions in mm. Not to scale.

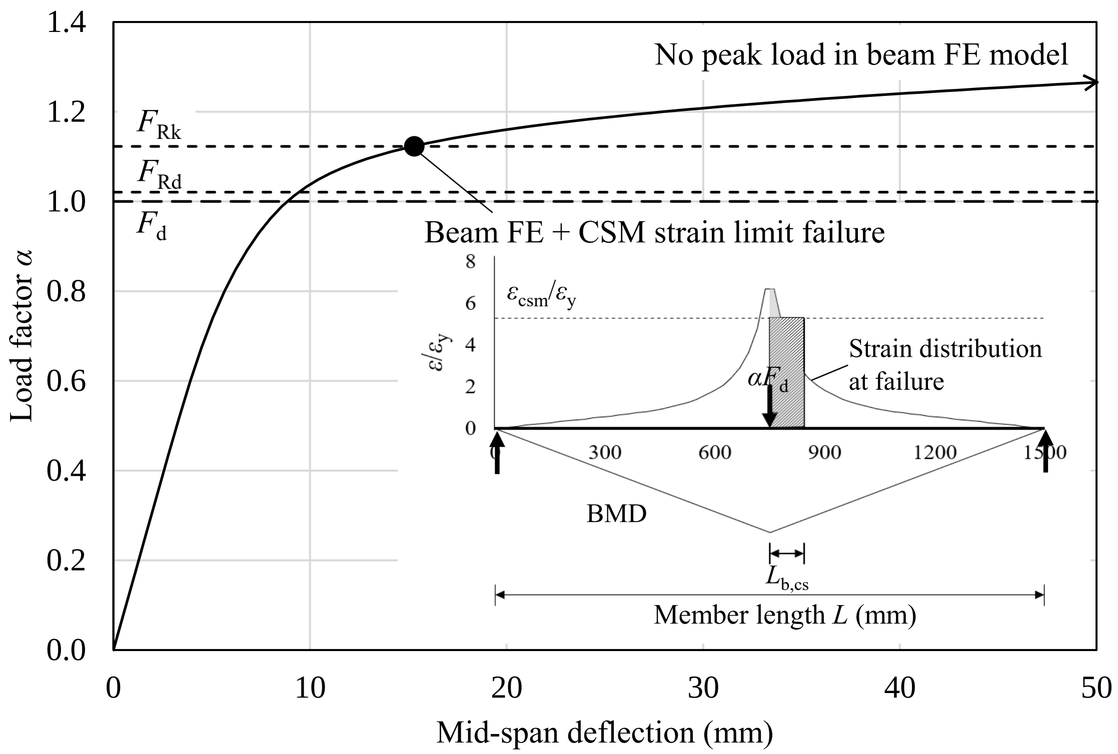

Figure 17: Worked example 1: Design of a duplex (f_y = 450 N/mm^2, E = 191000 N/mm^2) stainless steel RHS 200×100×5 beam under three-point bending.

HEB 140:

A = 4172 mm^2
I_{yy} = 14713403 mm^4
$W_{pl,y}$ = 238588 mm^3

L = 5600 mm
N_{Ed} = 48.2 kN
M_{Ed} = 52.4 kNm

f_y = 210 N/mm^2
f_u = 500 N/mm^2
E = 191000 N/mm^2
n = 7
m = 2.18
ε_u = 0.58

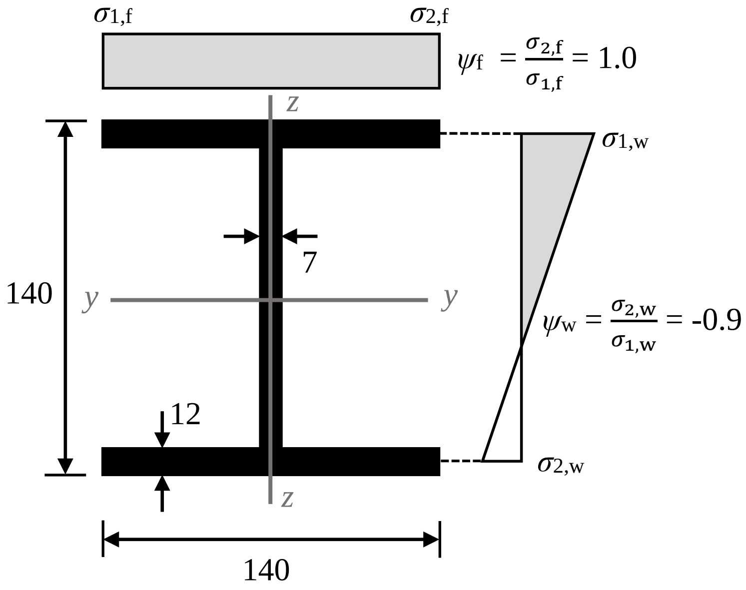

Figure 18: Worked example 2: HEB 140 cross-section under combined compression and major axis bending. All dimensions in mm. Not to scale. Note that ψ_w = -0.9 corresponds to the critical cross-section in the member.

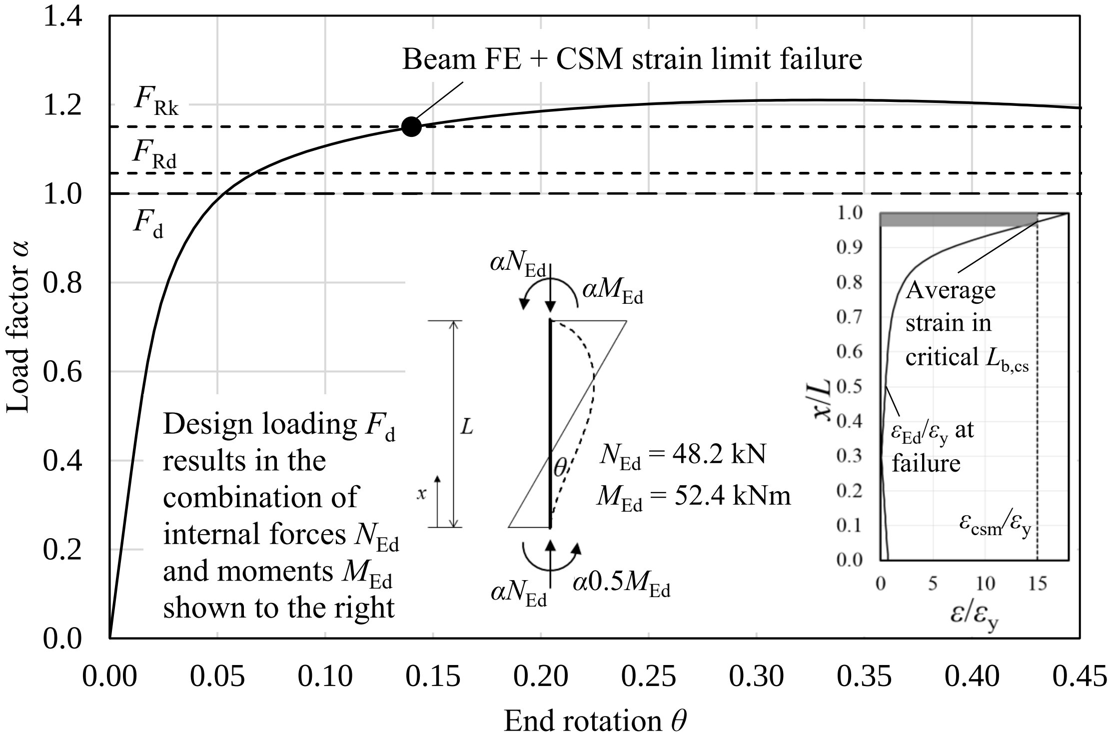

Figure 19: Worked example 2: Design of an austenitic (f_y = 210 N/mm^2, E = 191000 N/mm^2) stainless steel HEB 140 beam-column with $\bar{\lambda}$ = 1.0.

Table 1: Summary of shell FE model validation; comparison of the experimental and numerical ultimate capacities (FE/Test) for stainless steel I-section and SHS/RHS members under different loading conditions.

Member	Reference	Section	Grade	Loading	No. of tests	FE/Test Mean	FE/Test COV
Beams	Bu & Gardner [25]	I-section	Austenitic	3PB	4	1.01	0.022
				4PB	4	1.01	0.018
	Theofanous & Gardner [26]	SHS/RHS	Duplex	3PB	8	1.04	0.026
	Afshan & Gardner [27]	SHS/RHS	Ferritic	3PB	4	0.98	0.026
				4PB	4	1.02	0.049
Columns	Theofanous & Gardner [28]	SHS	Duplex	-	6	0.99	0.050
		RHS	Duplex	Major	3	0.94	0.092
				Minor	3	0.94	0.067
	Afshan & Gardner [27]	SHS	Ferritic	-	7	1.05	0.059
		RHS	Ferritic	Major	4	0.99	0.056
	Burgan, Baddoo, Gilsenan [29]	I-section	Austenitic	Major	6	0.99	0.039
				Minor	6	1.03	0.073
Beam-columns	Burgan, Baddoo, Gilsenan [29]	I-section	Austenitic	Major	8	1.02	0.032
	Bu & Gardner [30]	I-section	Austenitic	Major	6	0.99	0.057
				Minor	6	0.98	0.053
	Zhao, Gardner, Young [31]	SHS/RHS	Ferritic	Major	6	1.01	0.011
				Minor	6	0.93	0.021
				Total	91	1.00	0.057

Table 2: Two-stage Ramberg–Osgood material model parameters [42] used for parametric studies.

Cross-section	Grade	f_y (N/mm^2)	f_u (N/mm^2)	ε_u	n	m
I-sections	Austenitic	280	580	0.50	9.1	2.3
	Duplex	530	770	0.30	9.3	3.6
	Ferritic	320	480	0.16	17.2	2.8
Hollow section flats	Austenitic	460	700	0.20	7.1	2.9
	Duplex	630	780	0.13	7.5	4.8
	Ferritic	430	490	0.06	11.5	4.6
Hollow section corners	Austenitic	640	830	0.20	6.4	7.1
	Duplex	800	980	0.03	6.1	6.7
	Ferritic	590	610	0.01	5.7	6.8

Table 3: Summary of the resistance predictions determined using the proposed method M_{prop} and EN 1993-1-4 M_{EC}, normalised by the benchmark shell FE results M_{shell} for austenitic, duplex and ferritic stainless steel I- and hollow section members subjected to three- (3PB) and four- (4PB) point bending.

Section type	Load case	No.	M_{EC}/M_{shell}		$M_{prop(\Omega=15)}/M_{shell}$	
			Mean	COV	Mean	COV
I-section	3PB	267	0.73	0.066	0.92	0.078
	4PB	267	0.82	0.082	0.95	0.084
Hollow section	3PB	267	0.77	0.089	0.92	0.072
	Total	801	0.78	0.093	0.93	0.084

Table 4: Summary of the resistance predictions determined using the proposed method N_{prop} and EN 1993-1-4 N_{EC}, normalised by the benchmark shell FE results N_{shell} for austenitic, duplex and ferritic stainless steel I- and hollow section columns buckling about the major axis.

Section type	Grade	No.	N_{EC}/N_{shell}		N_{prop}/N_{shell}	
			Mean	COV	Mean	COV
I-section	Austenitic	225	1.00	0.036	0.92	0.032
	Duplex	150	0.92	0.049	0.94	0.034
	Ferritic	216	0.93	0.062	0.92	0.034
Hollow section	Austenitic	213	0.94	0.057	0.89	0.032
	Duplex	168	0.92	0.063	0.88	0.024
	Ferritic	213	0.89	0.064	0.86	0.045
	Total	1185	0.93	0.067	0.90	0.045

Table 5: Summary of radial resistance predictions for the three considered design methods: (i) Beam FE + CSM strain limit ε_{prop}, (ii) EN 1993-1-4 member checks $\varepsilon_{EC\text{-}trad}$ and (iii) GNIA + EN 1993-1-4 cross-section checks $\varepsilon_{EC\text{-}adv}$ relative to the benchmark shell FE results for austenitic, duplex and ferritic stainless steel hollow section beam-columns.

Member slenderness $\bar{\lambda}$	No.	ε_{prop}		$\varepsilon_{EC\text{-}trad}$		$\varepsilon_{EC\text{-}adv}$	
		Mean	COV	Mean	COV	Mean	COV
0.5	99	1.12	0.076	1.23	0.140	1.26	0.075
1.0	99	1.11	0.053	1.32	0.170	1.22	0.074
1.5	99	1.09	0.045	1.36	0.172	1.14	0.087
Total	297	1.11	0.061	1.30	0.167	1.21	0.088

Table 6: Summary of the statistical analysis results for the proposed design method assessed against the benchmark shell FE results for austenitic, duplex and ferritic stainless steel I- and hollow section members subjected to three- (3PB) and four- (4PB) point bending.

Section type	Load case	Grade	No.	$f_{y,mean}/f_{y,nom}$	V_{fy}	V_A	V_E	b	V_δ	γ_{M1}
I-section	3PB	Austenitic	89	1.3	0.060	0.022	0.03	1.095	0.061	0.98
		Duplex	89	1.1	0.030	0.022	0.03	1.138	0.041	1.02
		Ferritic	89	1.2	0.045	0.022	0.03	1.104	0.045	1.00
	4PB	Austenitic	89	1.3	0.060	0.022	0.03	1.051	0.034	0.99
		Duplex	89	1.1	0.030	0.022	0.03	1.116	0.041	1.05
		Ferritic	89	1.2	0.045	0.022	0.03	1.054	0.034	1.04
Hollow section	3PB	Austenitic	89	1.3	0.060	0.027	0.03	1.152	0.054	0.98
		Duplex	89	1.1	0.030	0.027	0.03	1.149	0.038	1.05
		Ferritic	89	1.2	0.045	0.027	0.03	1.117	0.038	1.01

Table 7: Summary of the statistical analysis results for the proposed design method assessed against the benchmark shell FE results for austenitic, duplex and ferritic stainless steel I- and hollow section columns buckling about the major axis.

Section type	Grade	$\bar{\lambda}$	No.	$f_{y,mean}/f_{y,nom}$	V_{fy}	V_A	V_E	b	V_δ	γ_{M1}
I-section	Austenitic	0.5	76	1.3	0.060	0.022	0.03	1.101	0.015	0.87
		1.0	76					1.080	0.048	0.96
		1.5	76					1.081	0.009	0.94
	Duplex	0.5	50	1.1	0.030	0.022	0.03	1.068	0.024	1.00
		1.0	50					1.072	0.033	1.03
		1.5	50					1.057	0.040	1.09
	Ferritic	0.5	72	1.2	0.045	0.022	0.03	1.070	0.027	0.95
		1.0	72					1.096	0.029	0.95
		1.5	72					1.095	0.038	1.02
Hollow section	Austenitic	0.5	71	1.3	0.060	0.027	0.03	1.083	0.024	0.90
		1.0	71					1.135	0.015	0.88
		1.5	71					1.155	0.011	0.91
	Duplex	0.5	56	1.1	0.030	0.027	0.03	1.111	0.032	0.98
		1.0	56					1.135	0.008	0.95
		1.5	56					1.145	0.007	0.98
	Ferritic	0.5	71	1.2	0.045	0.027	0.03	1.092	0.031	0.89
		1.0	71					1.187	0.010	0.82
		1.5	71					1.198	0.032	0.87

Table 8: Summary of the statistical analysis results for the proposed design method assessed against the benchmark shell FE results for austenitic, duplex and ferritic stainless steel hollow section beam-columns.

Grade	No.	$f_{y,mean}/f_{y,nom}$	V_{fy}	V_A	V_E	b	V_δ	γ_{M1}
Austenitic	99	1.3	0.060	0.027	0.03	1.079	0.021	0.93
Duplex	99	1.1	0.030	0.027	0.03	1.161	0.045	0.99
Ferritic	99	1.2	0.045	0.027	0.03	1.051	0.029	0.99